AD_____

Award Number: W81XWH-08-1-0636

TITLE: Premalignant Genetic and Epigenetic Alterations in Tubal Epithelium from Women with BRCA1 Mutations

PRINCIPAL INVESTIGATOR: Anton Krumm, Ph.D.

CONTRACTING ORGANIZATION: University of Washington
Seattle WA 98195

REPORT DATE: October 2010

TYPE OF REPORT: Annual

PREPARED FOR: U.S. Army Medical Research and Materiel Command
Fort Detrick, Maryland 21702-5012

REPORT DOCUMENTATION PAGE

Form Approved
OMB No. 0704-0188

1. REPORT DATE *(DD-MM-YYYY)*	2. REPORT TYPE	3. DATES COVERED *(From - To)*
10-14-2010	Annual	15 Sept 2009 – 14 Sept 2010

4. TITLE AND SUBTITLE
Premalignant Genetic and Epigenetic Alterations in Tubal Epithelium from Women with BRCA1 Mutations

5a. CONTRACT NUMBER

5b. GRANT NUMBER
W81XWH-08-1-0636

5c. PROGRAM ELEMENT NUMBER

6. AUTHOR(S)
Anton Krumm

Email: akrumm@u.washington.edu

5d. PROJECT NUMBER

5e. TASK NUMBER

5f. WORK UNIT NUMBER

7. PERFORMING ORGANIZATION NAME(S) AND ADDRESS(ES)

University of Washington
Seattle WA
98195-9472

8. PERFORMING ORGANIZATION REPORT NUMBER

9. SPONSORING / MONITORING AGENCY NAME(S) AND ADDRESS(ES)
U.S. Army Medical Research and Material Command
Fort Detrick
Maryland 21702-5012

10. SPONSOR/MONITOR'S ACRONYM(S)

11. SPONSOR/MONITOR'S REPORT NUMBER(S)

12. DISTRIBUTION / AVAILABILITY STATEMENT

Approved for public release; distribution unlimited

13. SUPPLEMENTARY NOTES
Ovarian Cancer, chromatin, DNA methylation, transcription factor binding, CTCF

14. ABSTRACT
Increasing evidence suggests that many types of ovarian cancers originate within the fallopian tube. The scope of this Translational Partnership project is to define a unique premalignant gene expression profile and to identify causal epigenetic relationships. As outlined in the statement of work, our analyses have identified a premalignant expression signature which potentially reflects early steps in ovarian carcinogenesis. While genes differentially expressed in BRCA1 normal Fallopian Tube epithelia and BRCA1 ovarian carcinoma were investigated in the Swisher lab, we have further established the proof-of-principle that demonstrates the role of DNA methylation of CTCF binding sites in cancer tissues. We gathered evidence that genes that are part of the premalignant signature are differentially methylated in ovarian cancer cell lines. DNA methylation analysis of isolated and pooled samples by laser-capture microscopy indicates that increased cytosine methylation at the CDKN1C gene may contribute to epigenetic changes that mark ovarian cancer.

15. SUBJECT TERMS
None provided.

16. SECURITY CLASSIFICATION OF:			17. LIMITATION OF ABSTRACT	18. NUMBER OF PAGES	19a. NAME OF RESPONSIBLE PERSON
a. REPORT	b. ABSTRACT	c. THIS PAGE			USAMRMC
U	U	U	UU	36	19b. TELEPHONE NUMBER *(include area code)*

Table of Contents

Premalignant Genetic and Epigenetic Alterations in Tubal Epithelium from Women with BRCA1 Mutations

OC073389 Final Report October, 14 2010

INTRODUCTION

Although it has been proposed that ovarian cancer originates from the surface epithelium of the ovary and/or the epithelial lining of ovarian inclusion cysts, there have been few reports of pre-neoplastic or early lesions at these sites. Instead, there has been increasing evidence that many ovarian cancers originate within the fallopian tube. Although the lifetime risk of ovarian cancer in the general population is 1-2%, women who inherit a mutation in the BRCA1 gene have up to a 50% lifetime risk of ovarian cancer. These high-risk women are frequently discovered to have occult neoplasms at the time of risk-reducing salpingo-oophorectomy, and 57-100% of these lesions are discovered in the fallopian tube. Our tissue bank included frozen fallopian tube tissue from women with BRCA1 mutations found to have occult fallopian tube carcinomas on final pathologic examination. We hypothesized that the histologically normal fallopian tube epithelium from these women would possess a unique gene expression profile which would reflect early disruptions in gene expression contributing to the development of carcinoma.

BODY

In the first year, we completed the work outlined in our statement of work with minor modifications. The objective of the first year was to complete laser capture microdissection, RNA preparation and amplification and expression array analyses for BRCA1 ovarian cancers, fallopian tube epithelium (FTE) from women at normal risk of ovarian cancer and FT from women with BRCA1 mutations, then obtain a list of candidate genes that may contribute to early ovarian carcinogenesis (Figure 1 and attached manuscript). We have completed that objective as detailed below. We originally planned to do 60 samples. However, due to the markedly decreased budget we were unable to complete analyses on that many samples and reduced our work to a total of 48 samples. This allowed us to achieve our objective while retaining adequate funds to carry out the epigenetic work outlined for Year 2. Quantitative RT-PCR was used to confirm array results for a subset of genes in the premalignant expression signature (Figure 2). The work for Year 1 was performed in the Swisher lab as planned. Results were summarized in the October 2009 progress report and have been accepted for publication in Neoplasia. That manuscript is attached to this report.

Changes in the methylation status of DNA have the potential to serve as an early detection marker for malignancies. Previous work in several labs including ours has revealed that epigenetic aberrations including methylation of CTCF target sites are a key event in carcinogenesis [[1], reviewed in [2]]. CpG methylation of CTCF target motifs inhibits binding of CTCF and permits spreading of DNA methylation and subsequent silencing of genes such as tumor suppressor genes [3]. To test the epigenetic contribution to the malignant transformation in the ovary, we pursued two objectives: (1), determine a role for DNA methylation and CTCF binding in the deregulation of specific genes including those identified by the Swisher lab and (2), evaluate and validate the contributions of alterations in DNA methylation and CTCF binding.

The epigenetic analyses were performed in the Krumm lab and the Swisher lab identified tissue samples and performed laser capture microdissection to obtain DNA samples on 40 normal FT and

malignant samples. The Krumm laboratory has requested a no cost extension to complete the epigenetic analyses which are ongoing. FTE and ovarian carcinomas were obtained from an IRB approved tissue bank. Laser capture microdissection (LCM) of formalin fixed, paraffin embedded sections was used to isolate neoplastic cells or histologically normal FTE. Total DNA was obtained using the Picopure DNA isolation kit (Arcturus).

Because the exact role for DNA methylation in controlling CTCF binding is poorly defined, we first examined the contribution of individual cytosine residues to binding of CTCF at several genomic loci. CTCF binding sequences derived from several genes including the human MYC oncogene as well as the IGF2 gene and the IGF2BP1 gene were tested for their ability to recruit CTCF in vitro using immobilized template assays (Figure 3). DNA templates either methylated or unmethylated were linked to magnetic beads, incubated with nuclear extract, washed, and tested for association with CTCF by western blotting. As shown in Figure 3B, templates containing wildtype CTCF binding sequences derived from the IGF2BP1 gene (IGF2BP1 wt, lower panel of Figure 3B) efficiently recruit CTCF. In contrast, CTCF binding was severely reduced when the target motifs were mutated by three base substitutions (IGF2BP1 mut, Figure 3B). To establish whether binding of CTCF to its target motifs is inhibited by cytosine methylation, we tested immobilized templates after SspI-mediated methylation of cytosine residues *in vitro*. We examined CTCF motifs containing different CpG content such as the myc site A [3] as well as the B1 sequence of the ICR of the human IGF2/H19 locus [4]. Cytosine methylation at the human B1 sequence is known to inhibit binding of CTCF [4]. Consistent with this, recruitment of CTCF to immobilized templates containing the B1 sequence or the myc site A is highly sensitive to DNA methylation. (Figure 3A, upper panel). In contrast, CpG methylation of the IGF2BP1 motif has no effect on CTCF recruitment. Replacement of the IGF2BP1 core motif by the CTCF-binding sites of the chicken FII insulator element yields similar results. However, CTCF binding becomes sensitive to CpG methylation upon modification of the core motif into human B1 sequence. In combination, our experiment indicate that the inhibition of CTCF binding is not only dependent on DNA methylation but is also dependent on additional features of the motif including the number and position of cytosine residues. These results will refine our ability to locate sites genome-wide that are regulated through methylation of CpG residues.

To further investigate a role for cytosine methylation in the inhibition of CTCF binding and deregulation of gene expression, we tested several sites at the HOX gene locus *in vivo* in cancer cell lines established from ovarian, breast and prostate tissue (Figure 4). The HOXA gene cluster is a family of homeotic genes that encode transcription factors frequently inactivated in cancer cell types.
The HOX gene domain contains several CTCF sites (hx1-hx5) previously identified in our ChIP-Chip analysis in the breast epithelial cell line HBL100. Importantly, CTCF binding at hx1 is absent in the prostate epithelial cell line PC3 [5]. Genomic sequencing of the hx1 region revealed complete sequence identity at this site in HBL100 and PC3 cells, suggesting that epigenetic mechanisms account for the loss of CTCF binding in PC3 prostate cancer cells. Using a combination of methylation-sensitive restriction enzymes and PCR we analyzed the level of DNA methylation in the ovarian cancer cell line A2780 and compared it to the prostate cancer cell lines PC3 and C4-2. These experiments identified DNA methylation at the hx1 binding site in A2780 and PC3 cells but not in HBL100 cells and C4-2 cells. Most importantly, these studies further confirm a correlation of DNA methylation and loss of CTCF binding; while hx1 in the prostate cell line C4-2 is both unmethylated and bound by CTCF, hx1 in the A2780 and PC3 cell lines is methylated and not bound by CTCF. These data further support our hypothesis that epigenetic mechanisms and loss of CTCF binding contribute to reprogramming of gene expression during disease progression.

To address the potential role of CTCF binding and DNA methylation in deregulation of those genes identified by the Swisher lab, we scanned the genomic regions harboring candidate genes for known CTCF binding sites. Importantly, the majority of candidate genes are associated with one or more CTCF sites in a sequence space of 100 kb surrounding candidate loci. For only six loci is the closest CTCF binding site located more than 100 kb away. The distribution of CTCF sites across the subset of premalignant signature genes is similar to the distribution found genome-wide: About one half of CTCF sites are located in intergenic regions, with an average distance of approximately 47 kb. About 20% CTCF sites are located at transcription start sites, and 34% are located within introns and exons. Three examples of loci with CTCF binding sites in the vicinity of the genes under study are shown in Figure 5.

To obtain initial data on differential binding of CTCF at premalignant signature genes, we performed methylation-sensitive PCR on genomic DNA from several cancer cell lines including the ovarian cancer cell line OVCAR3. This analysis takes advantage of the methylation-sensitive restriction enzyme AciI that digests only unmethylated genomic regions, eliminating templates for subsequent PCR. Thus, while unmethylated regions yield no PCR product, methylated regions are protected from restriction digest and produce amplified DNA fragments. Using this approach, we investigated the methylation status at PAK3, JAG1, and LOC388798 gene loci. As shown in Figure 6 and 7, the CTCF binding region in PAK3 is methylated in the ovarian cancer cell line OVCAR3 but is un-methylated in the prostate cell line LnCaP. In contrast, our analyses at the LOC388798 on chromosome 20 revealed that this region is unmethylated in all cell lines tested.

Our technical objective 2 originally included methylation analysis using methylated DNA immunoprecipitation (MeDIP) and microarrays tiling through gene loci differentially expressed between normal tubal epithelium and BRCA1 carcinomas. However, our previous experience indicated that this approach limited our ability to quantify methylation levels. Moreover, while other approaches including extensive bisulfite sequencing can quantitatively reveal differential methylation between normal and tumor cells, these methods do not permit DNA methylation analyses at a high-throughput level. To accommodate highly quantitative and efficient analyses of methylation at differentially expressed gene loci, we employed EpiTYPER, a quantitative DNA methylation analysis using the MassARRAY® system. This approach combines bisulfate-mediated base-specific cleavage of methylated DNA and matrix-assisted laser desorption/ionization time-of-flight mass spectrometry (MALDI-TOF) previously introduced for SNP discovery. This approach includes a PCR step in which bisulfite-treated genomic DNA is amplified with primers containing a T7 promoter sequences. After transcribing DNA by T7 polymerase, RNA is cleaved in a base-specific manner and analyzed by MALDI-TOF mass spectrometry. This approach generates quantitative results for each cleavage product with a standard deviation of 5%, an important feature and precision that is not available with MeDIP-Chip analyses. Moreover, the EpiTYPER platform is capable of detecting methylation levels as low as 5% in sample mixtures and is thus highly sensitive and useful for the precise characterization of epigenetic changes in cancer phenotypes.

A very important step in epigenetic analyses using the EpiTYPER technology is the selection of PCR primers and the establishment of robust PCR conditions. Treatment of DNA with sodium bisulfate results in the complete transformation of unmethylated cytosines to uracil. The chemically converted cytosines are amplified by PCR as thymines. Analysis of these PCR products reveals the initial methylation profile of the region of interest. A technical advantage of the method resides in the use of PCR, which allows for analysis of samples with very low DNA content. However, PCR amplification can often be the most difficult with the challenge residing in the specific amplification

of bisulfite-treated DNA. High redundancy of the target sequences as reflected by the original G/C richness creates long stretches of thymines, which are often difficult for polymerases to faithfully replicate. Moreover, DNA fragmentation during bisulfate treatment leads to an empirical upper size limit of the PCR amplicon of 400–500 bp. Indeed, only short amplicons are amplified and the need for nested primers and a second round of PCR is often necessary.

To overcome these technical challenges, primer design is crucial since dimer formations are greatly facilitated by the T/A richness of the sense and antisense oligos, respectively. Moreover, primers designed for bisulfite-treated templates frequently generate non-specific PCR products because of mispriming in the highly redundant genome generated by bisulfate treatment. Although several primer-design algorithms exist for amplification of bisulfite-treated DNA the identification of reliable primer combinations remains difficult.

Primer design coupled with DNA degradation during tissue fixation/extraction and bisulfite treatment challenge efficient amplification. Thus, we have spent a significant amount of effort both to establish experimental conditions that limit DNA degradation and to select primer pairs that efficiently amplify the targeted genomic region. We selected five genes of particular biologic interest. Three of these genes, JAG1, PDGFC, and CDNK1C were down regulated in the premalignant signature while THOC3 and LOC388796 were up regulated. For each gene, we designed primers to interrogate the methylation status of the promoter and associated CTCF binding sites. A total of 16 amplicons were evaluated with initial optimization results shown in Table 1. The primer analysis using the Agilent Bioanalyzer is shown for a subset of amplicons in Figure 8.

Amplicon:		Optimization 1		Optimization 2		Optimization 3		Optimization 4			
	Expected size	Controls	LCMs	Controls	LCMs	Controls	LCMs	Controls	LCMs	Temps.	Notes
CDKN1C-promorer 1	259	Y	N	Y	N	N	N	Y	N (PD)	58, 56, 54	Re-design
CDKN1C-promoter 2	402	Y	N	Y	N (PD)	N	N	Y	N (PD)	58, 56, 54	Re-design
CDKN1C-promoter 3	282	N	N	N	N	Y	N	Y (PD)	N (PD)	58, 60, 58-1ul, 56-1ul	Re-design
CDKN1C-CTCF	408	Y	N	Y	N	N	N	Y	N	58, 56, 54	Re-design
JAG1-promoter 1	408	Y	N (PD)	-------	-------	-------	-------	-------	-------	58	Re-design
JAG1-promoter 2	357	N	N	N	N	N	N	-------	-------	58, 56, 54	Re-design
JAG1-CTCF 1	225	Y	Y	-------	-------	-------	-------	-------	-------	58	Run at 58ºC
JAG1-CTCF 2	144	Y	Y	-------	-------	-------	-------	-------	-------	58	Run at 58ºC
PDGFC-CTCF	212	Y	Y	-------	-------	-------	-------	-------	-------	58	Run at 58ºC
PDGFC-promoter	292	N	N	N	N	Y	N (PD)	-------	-------	58, 60, 58-1ul	Re-design
LOC-CTCF 1	312	N	N	N	N	Y	N, Y	Y	N	58, 60, 58-1ul, 56-1ul	Re-design
LOC-CTCF 2	294	N	N	N	N	N	N	Y	N	58, 60, 58-1ul, 56	Re-design
LOC-5' UTR 1	391	Y	N (PD)	Y	N (PD)	N	N	-------	-------	58, 56, 54	Re-design
LOC-5' UTR 2	275	Y	Y	N	N	-------	-------	-------	-------	58, 60	Run at 58ºC
THOC3-CTCF	220	Y	Y	-------	-------	-------	-------	-------	-------	58	Run at 58ºC
THOC3-promoter	489	Y	N	-------	-------	-------	-------	-------	-------	58	Re-design

Table 1. Results of optimization using the EpiTYPER platform. Amplicons spanning the promoters and associated CTCF binding sites for five genes were evaluated. In some instances, 2 or 3 amplicons were designed to ensure interrogation of the methylation status of the entire promoter and/or CTCF binding domain. Highlighted in blue are the five amplicons that were successful in the first round of optimization and were also successful with LCM material. Generally, amplicons worked well with the control samples (no LCM captured DNAs), but failed with the laser capture samples. Successful amplicons ranged in size from 144-275bp, while unsuccessful amplicons ranged in size from 259-489bp. PD, primer dimer/non specific amplification.

Successful amplicons were then used to quantitatively determine the methylation status of individual CpGs in a small series of ovarian cancer (3) and normal samples (2). These results are shown in Figure 10.

Given the amount of effort and time required to design and optimize primer conditions, our next round of optimization and validation focused on CDNK1C. CDKN1C (p57/Kip2) is an imprinted (maternally expressed) cell cycle regulatory gene on chromosome 11p15.4. Importantly, disruption of CDKN1C expression causes the cancer predisposing syndrome Beckwith-Wiedemann. CDKN1C has also been implicated as a tumor suppressor gene in a number of human malignant neoplasms including breast, lung, pancreatic, bladder, esophageal and a variety of hematological and myeloid neoplasms. While CDKN1C dysregulation has not been extensively studied in ovarian carcinoma, the majority (75%) of sporadic ovarian carcinomas demonstrate reduced CDKN1C protein expression (<10% of tumor cells) using IHC. Thus it is important to understand the mechanism responsible for reduced expression of CDKN1C in ovarian carcinomas.

Previously data added to the UCSC Genome Browser revealed additional putative CTCF binding sites at the CDKN1C locus ((CDKN1C_01 to _04, Figure 9) Given the biological significance of the potential regulatory sites, primers were designed to allow for the evaluation of methylation status of these four CTCF binding domains as well as LOC388796 5'UTR 1 since the other amplicon LOC388796 5'UTR 2 indicated differential methylation (see Figure 11). A summary of primer optimization results in shown in Table 2.

		Optimization 1		Optimization 2		Optimization 3			
Amplicon:	Expected size	Controls	LCMs	Controls	LCMs	Controls	LCMs	Temps.	Notes
CDKN1C_01	224	N (PD)	N (PD)	N (PD)	N (PD)	-------	-------	58°, 56°	Re-design
CDKN1C_02	300	Y/N	Y	Y	Y	-------	-------	58°	Good. Run at 58°
CDKN1C_03	335	Y	Y	-------	-------	-------	-------	58°	Good. Run at 58°
CDKN1C_04	222	Y/N (PD)	N (PD)	Y (PD)	Y/N (PD)	Y/N (PD)	Y/N (PD)	58°, 60°, 62°	Re-design
LOC-5' UTR 1	190	Y	Y/N	Y	Y	-------	-------	58°, 56°	Good. Run at 56°

Table 2. Results of optimization using the EpiTYPER platform. Amplicons spanning the four putative CDKN1C-associated CTCF binding sites as well as the 5'UTR of LOC388796 were evaluated. Highlighted in blue are the three amplicons that were successful in this round of optimization which were also successful with LCM material. PD, primer dimer/non specific amplification.

Successful amplicons were then used to quantitatively determine the methylation status of individual CpGs in a small series of ovarian cancer (3) and normal samples (2). These results are shown in Figure 11.

KEY ACCOMPLISHMENTS

The comparison of WT-FTE vs B1-FTE resulted in 152 differentially expressed probe sets and the comparison of WT-FTE vs B1-OC resulted in 4079 differentially expressed probe sets. The overlap between these 2 lists included 29 concordant down-regulated probe sets, 12 concordant up-regulated probe sets, and 7 probe sets showing discordance. The overlap of 41 of 152 probe sets was statistically highly significant and therefore not attributable to chance. The 41 concordant probe sets compose the premalignant signature (see attached manuscript). Down-regulated genes in the premalignant signature included several known tumor suppressor genes such as CDKN1C and

EFEMP1. Up-regulated genes included several thought to be important in invasion and metastasis such as E2F3. qRT-PCR confirmed array results for EFEMP1, p57, CYP3A5, and CSPG5 in a subset of samples.

Our epigenetic studies further refined and confirmed evidence for antagonistic action of DNA methylation and CTCF binding at several loci. Our data demonstrate the influence of specific DNA methylation patterns on CTCF binding at several genomic loci including the HOX genes. To quantitatively define changes in cytosine methylation in genes that constitute the premalignant signature for ovarian cancer, we established the experimental protocol for the EpiTYPER analyses. Importantly, our survey of cytosine methylation in a small subset of normal and tumor tissues indicates an increase in DNA methylation at the CDKN1C tumor suppressor gene and the 5'UTR of LOC388796. To confirm the significance of this observation, we have prepared DNA from an additional 40 microdissected samples of which 15 are derived from fallopian tubal epithelium and 25 are from ovarian epithelium (sporadic, BRCA1 or 2 positive). The Krumm lab has requested a no-cost extension to allow for completing this analysis.

REPORTABLE OUTCOMES

A manuscript on the expression data is currently in press at Neoplasia. The uncorrected proof is attached.

CONCLUSION

By comparing the histologically normal FTE from women who carry BRCA1 mutations and have micro-invasive foci with normal FTE from women without BRCA1 mutations, we have identified a premalignant expression signature which may reflect early steps in BRCA1-mediated ovarian carcinogenesis. The significant overlap in genes differentially expressed between BRCA1 normal FTE and BRCA1 ovarian carcinomas confirms that our relatively high risk approach has paid off. We have used histologically normal BRCA1 FT near an identifiable neoplastic FT lesion to identify alterations in gene expression profiles that contain the same as expression differences in BRCA1 ovarian carcinomas.

Our preliminary epigenetic analyses did not detect any differences between BRCA1 cancers and normal risk FTE for JAG1 at both CTCF sites 1 and 2, the THOC3 CTCF site, the PDGFC CTCF site and amplicon 1 of the 5'UTR of LOC388796 (amplicon 1; Figure 10). However, our initial quantitative methylation analyses indicate differences in methylation at amplicon 2 of 5'UTR of LOC388796 (amplicon 2; Figure 10) and two of the CTCF sites associated with CDNK1C (CDNK1C-02, and -03; Figure 11).

Given the potential biological impact of loss of CDKN1C expression in ovarian carcinomas and our finding that in some the mechanism responsible for reduced expression may be methylation of associated CTCF binding domains, we have recently optimized primers spanning CTCF site CDKN1C-01 (Figure 9). Thus, additional time has been required to design primers and optimize PCR conditions for CDKN1C-associated CTCF binding domains. We are now preparing to perform a detailed methylation mapping of CDKN1C CTCF sites in an additional 40 microdissected samples including 15 from fallopian tubal (FT) epithelium (7 normal, 7 FT occult cancer, 1 BRCA1+ ovarian cancer), and 25 from ovarian epithelium (8 BRCA1+ ovarian cancer, 5 BRCA2+ ovarian cancer and 12 sporadic ovarian cancer).
We anticipate those data will be submitted as a manuscript in 2011.

REFERENCES:

1. Witcher, M. and B.M. Emerson, *Epigenetic silencing of the p16(INK4a) tumor suppressor is associated with loss of CTCF binding and a chromatin boundary.* Mol Cell, 2009. **34**(3): p. 271-84.
2. Phillips, J.E. and V.G. Corces, *CTCF: master weaver of the genome.* Cell, 2009. **137**(7): p. 1194-211.
3. Gombert, W.M. and A. Krumm, *Targeted deletion of multiple CTCF-binding elements in the human C-MYC gene reveals a requirement for CTCF in C-MYC expression.* PLoS One, 2009. **4**(7): p. e6109.
4. Hark, A.T., et al., *CTCF mediates methylation-sensitive enhancer-blocking activity at the H19/Igf2 locus.* Nature, 2000. **405**(6785): p. 486-9.
5. Rubio, E.D., et al., *CTCF physically links cohesin to chromatin.* Proc Natl Acad Sci U S A, 2008. **105**(24): p. 8309-14.

SUPPORTING DATA

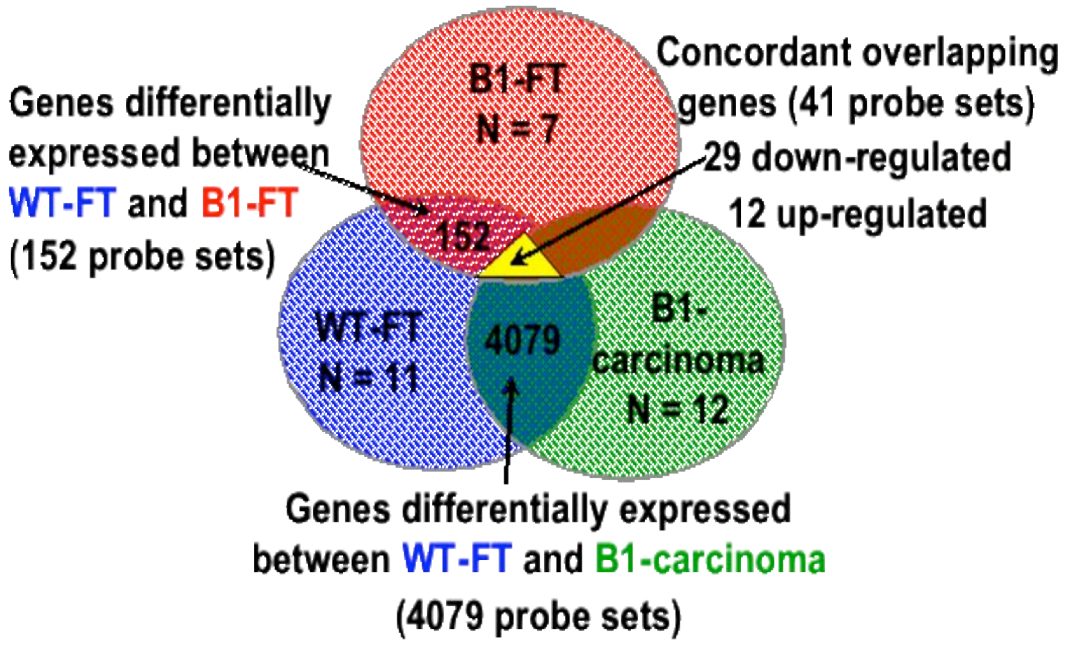

Figure 1. Diagram illustrating the protocol used to define the gene signature: Pairwise comparison between the WT-FT group and the B1-FT group (fold change ≥1.8, p-value <0.01) identified 152 differentially expressed probe sets. Pairwise comparison between the WT-FT group and the B1-carcinoma group (fold change ≥1.8, p-value <0.01) identified 4079 differentially expressed probe sets. To minimize the false discovery rate probe sets were only included in the gene signature with concordant down-regulation or up-regulation in both pairwise comparisons. The 41 probe sets fulfilling this criteria are shown in the Table 1.

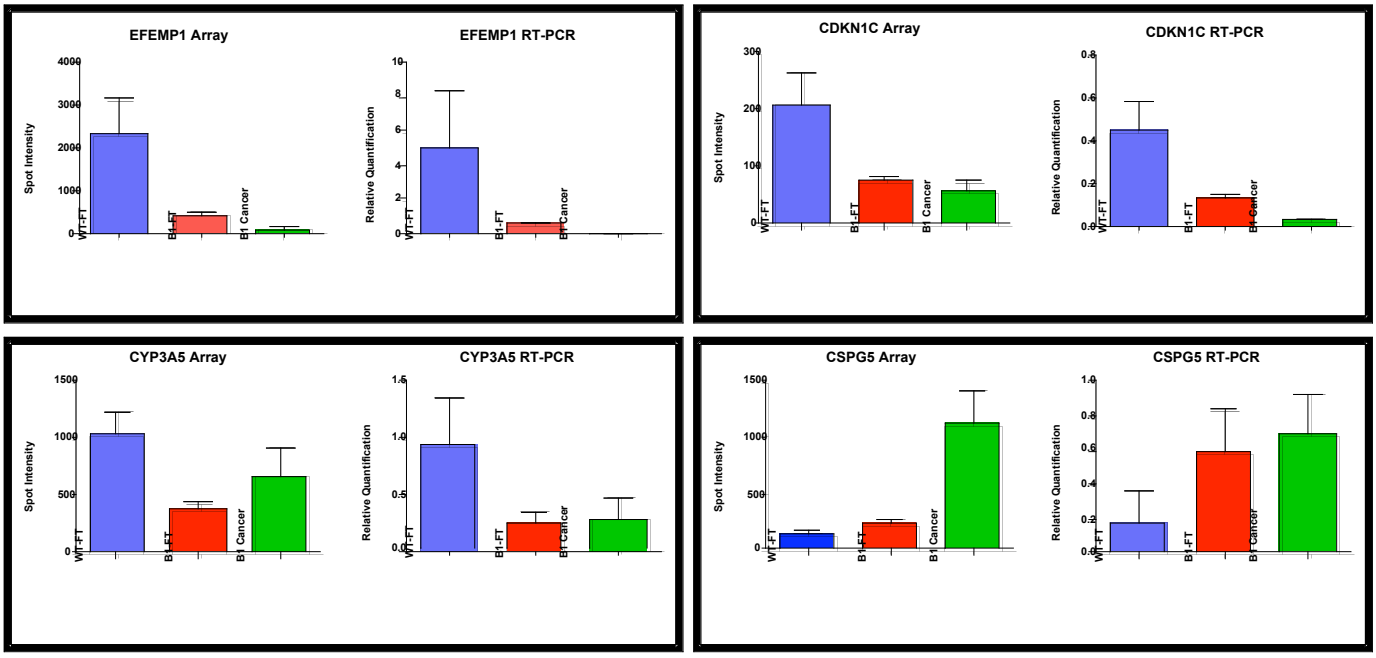

Figure 2. Real-time RT-PCR results: Four genes from the gene signature were selected for validation by RT-PCR with Taqman assays, using five cases from each group. EFEMP1 (EGF-containing fibulin-like extracellular matrix protein 1), CDKN1C (Cyclin-dependent kinase inhibitor 1C or p57), CYP3A5 (Cytochrome p450, family 3, subfamily A), and CSPG5 (Chondroitin sulfate proteoglycan 5 or neuroglycan C). Array corresponded well with RT-PCR results as shown.

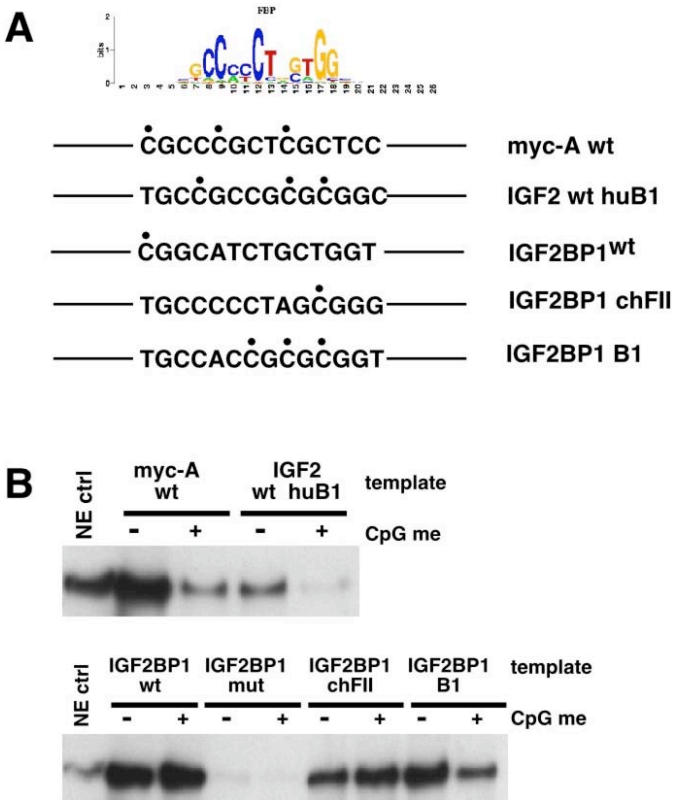

Figure 3: Methylation sensitive binding of CTCF to its target sequences. (A) CTCF target motifs derived from the MYC, IGF2, and IGF2BP1 gene loci were tested for their ability to bind CTCF in their unmethylated and methylated form. Methylable cytosine residues are indicated by filled circles. (B) Western blots reveal the amount of CTCF bound to the target motifs. Binding of CTCF to myc-A and IGF2 huB1 is significantly inhibited by methylation (+ CpG me). In contrast, methylation of the IGF2BP1 target motif does not affect recruitment of CTCF (compare IGF2BP1wt +/- CpGme). Modification of the IGF2BP1 target sequence into a motif that resembles that of the IGF2 gene (IGF2BP1 B1) restores the methylation sensitivity of CTCF binding. NE ctrl represents signal obtained from nuclear extract.

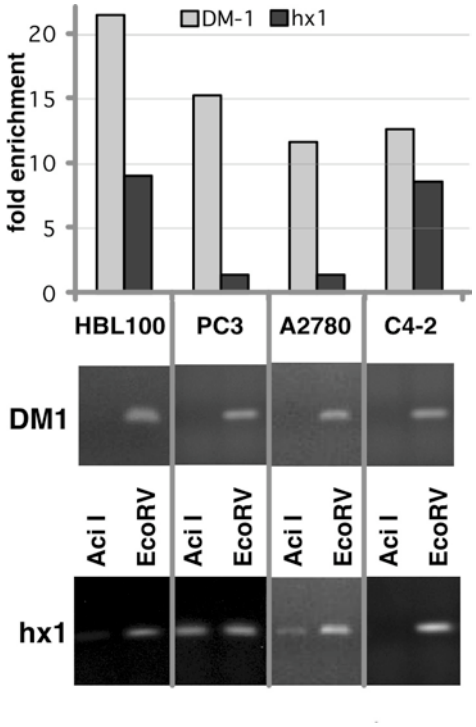

Figure 4. DNA methylation-sensitive binding of CTCF at the HoxA locus. Upper panel, enrichment of CTCF bound sequences at the DM1 locus (grey bars) and the hx1 binding site (black bars) in ChIP in breast epithelial cell type HBL100, ovarian cancer cell line A2780, and prostate cancer cell lines PC3 and C4-2. While CTCF is bound to the DM1 locus in all cell lines (grey bars), it fails to bind to the hx1 site at the HoxA gene domain in PC3 and A2780 (black bars). Lower panel, DNA methylation analysis by PCR of genomic DNA after restriction digest with methylation-sensitive Aci I or Eco RV (control digest; amplicons do not contain Eco RV sites) reveal no DNA methylation at DM1 (no PCR product due to digest of DNA). In contrast, hx1 in PC3 and A2780 is methylated, leading to inhibition of CTCF binding.

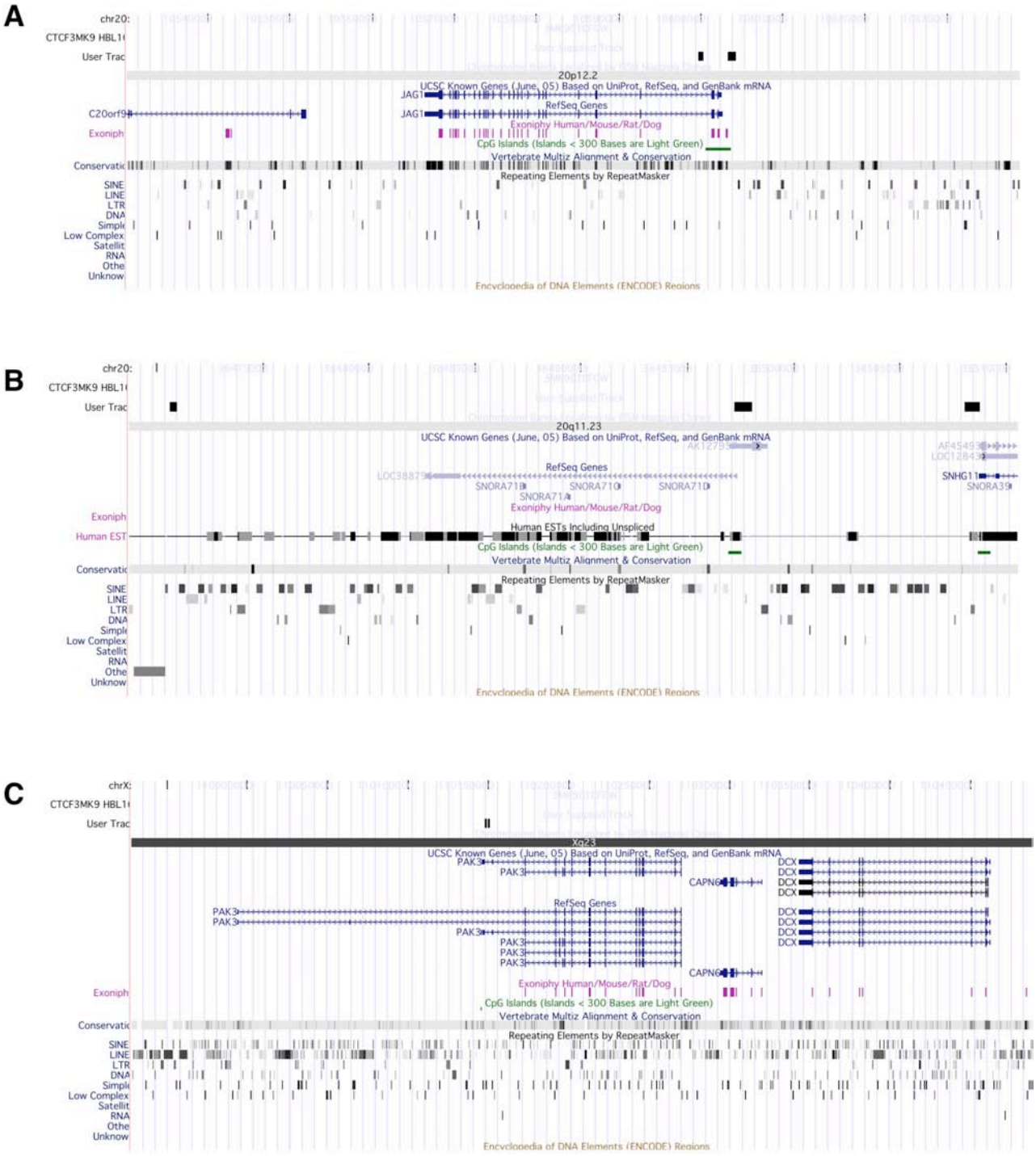

Figure 5. Distribution of CTCF sites at genomic loci that are differentially expressed and part of the premalignant gene signature. Custom tracks of the UCSC genome browser of the JAG1 (A), LOC38879 (B), and PAK3 (C) genes are shown as examples. CTCF binding regions are indicated by black boxes within "User track". Chromosome and position are shown at the top.

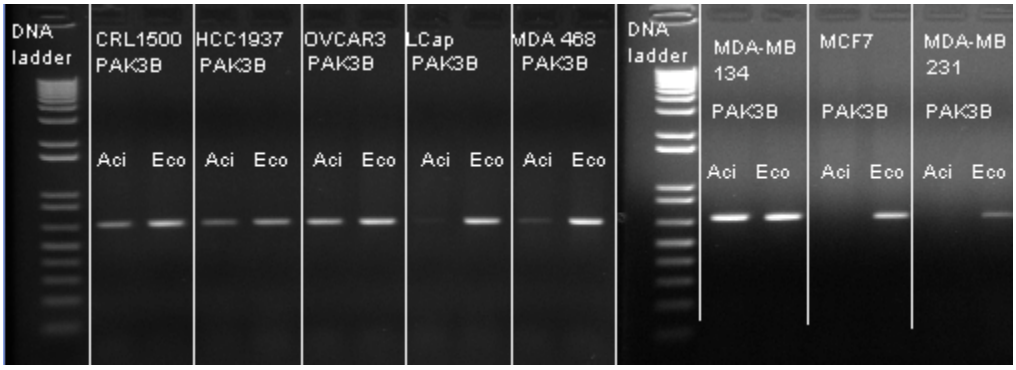

Figure 6. Differential methylation of CTCF binding sites at the PAK3 gene locus in several cancer cell lines. Genomic DNA isolated from indicated cell types was digested with AciI (CpG methylation sensitive) or EcoRV (control). Genomic region of PAK3A gene was subsequently amplified by PCR. CpG methylation at CTCF binding region blocks digest by AciI, and permits amplification of PAK3B region (e.g. ovarian cancer cell line OVCAR3 and breast cancer cell line MDA-MB134). In contrast, non-methylated PAK3 regions are digested in the presence of AciI, and PCR amplification does not yield any product (e.g. prostate cancer cell line LnCaP).

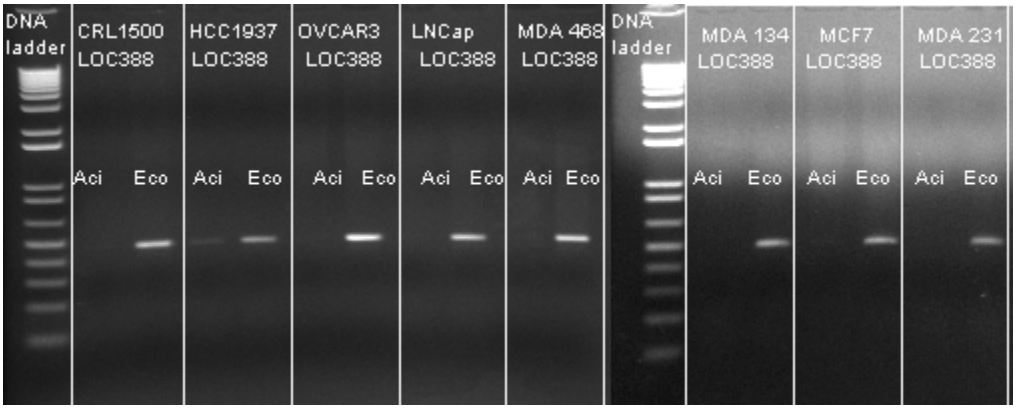

Figure 7. CTCF binding region at LOC388796 is invariably unmethylated in different tissues/cell lines (CRL1500, HCC1937, OVCAR3, LnCaP, MDA468, MDA-MB134, MCF7, and MDA-MB231). Genomic DNA digested with either AciI or EcoRV was amplified with primers specific for a CTCF binding region at LOC388796 (chr20). Absence of PCR product using genomic DNA digested by AciI indicates absence of methylation in all cell lines.

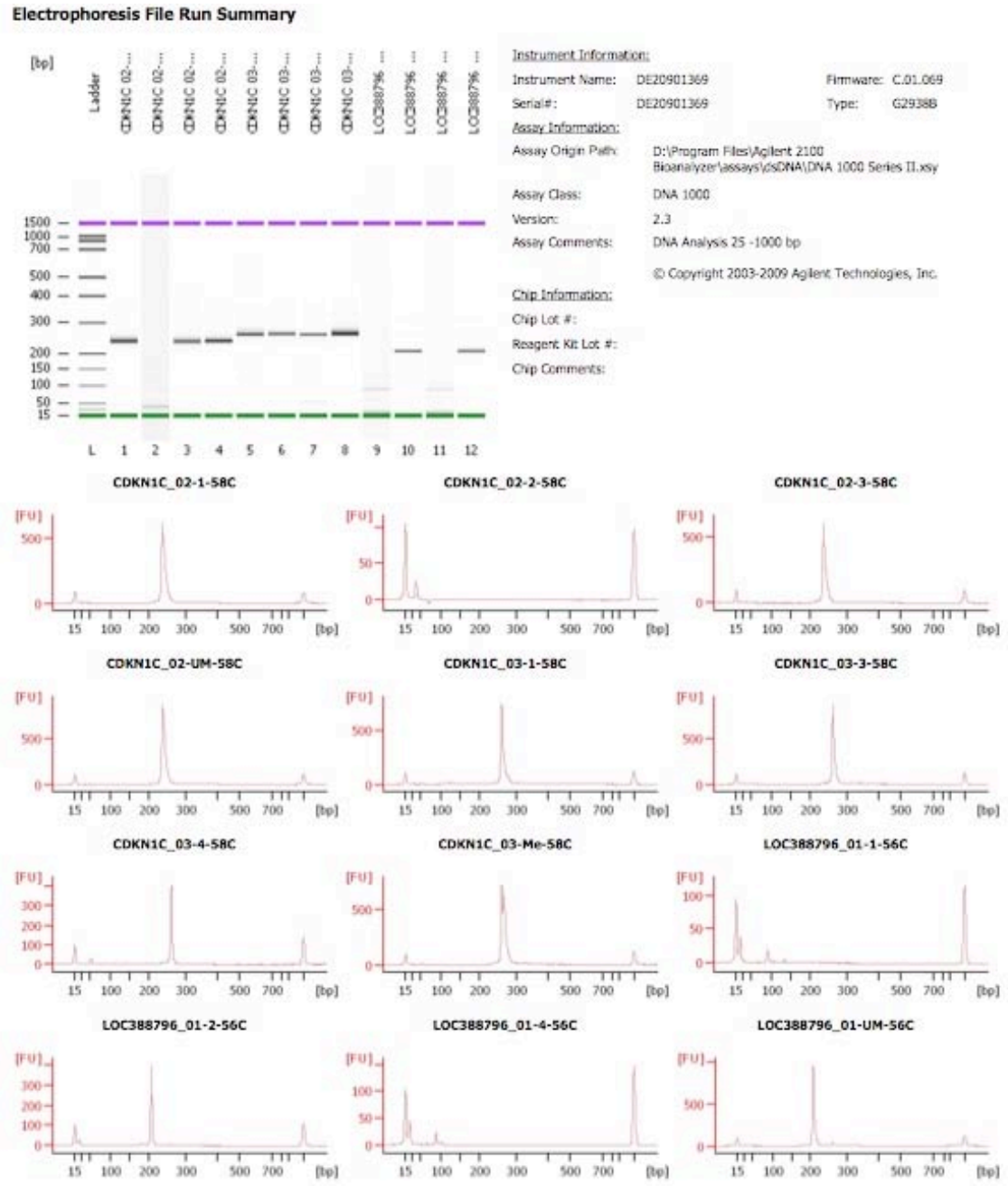

Figure 8: Example of primer optimization and analysis with the Bioanalyzer to identify primer combinations suitable for EpiTYPER assay. Several primer combinations were used to amplify genomic regions by PCR. Amplicons were analyzed using the Agilent 2100 Bioanalyzer. Top panel, electrophoresis of amplicons. Position of references are indicated by purple and green bands. Quantitative analyses of each of the PCR products is shown below.

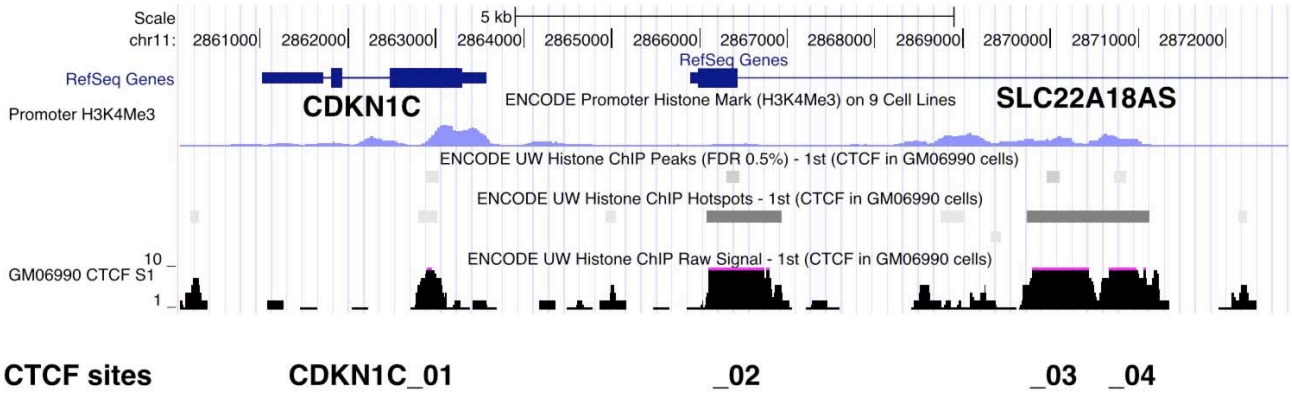

Figure 9: Distribution of CTCF sites across the CDKN1C genomic region on chromosome 11. Position of CTCF sites 1 to 3 in the GM6990 cell line relative to the position of the CDKN1C and SLC22A18AS genes are shown.

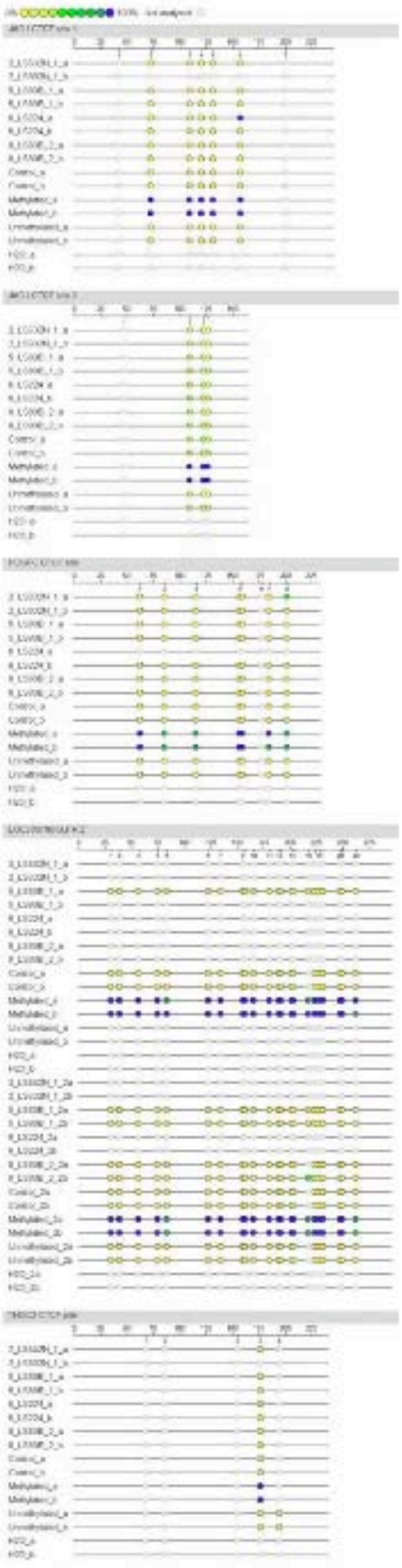

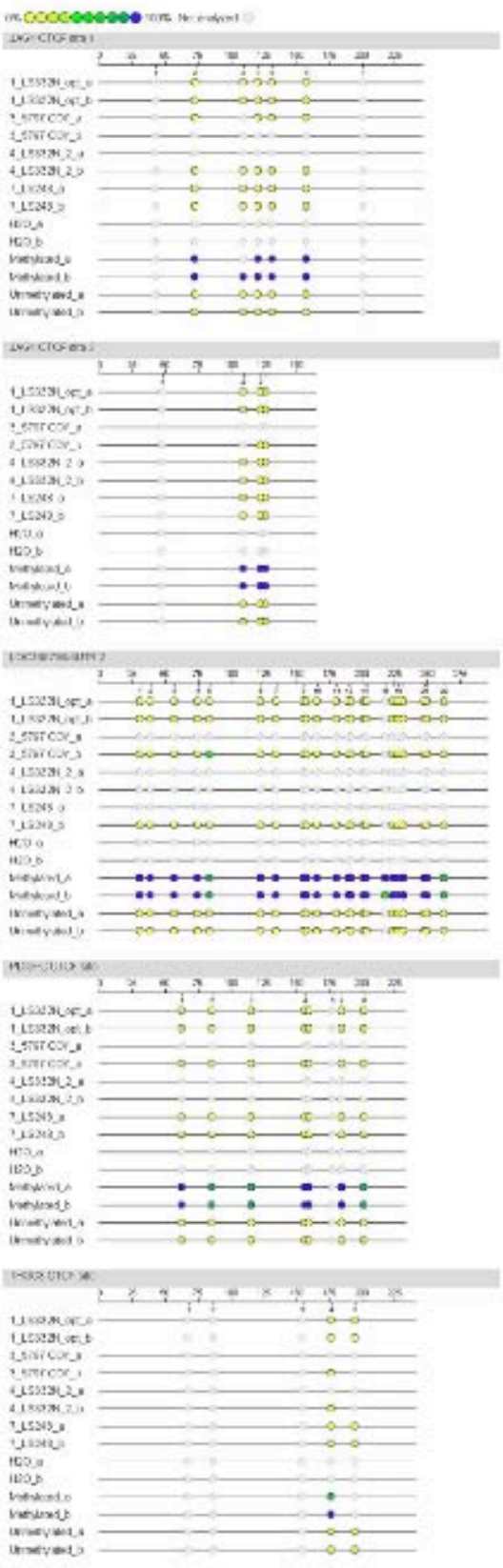

Figure 10: Quantitative DNA methylation analysis in ovarian cancers and normal ovarian epithelium for CTCF sites associated with JAG1, PDGF, THOC3 and the 5'UTR of LOC388796. LCM captured DNA from three ovarian cancers (LS80B, LS224, and LS240) and two normal samples (LS332N and 5797 COY) was treated with sodium bisulfite. Converted DNAs were amplified with primers spanning CTCF binding sites or promoter regions for the indicated genes. PCR products were then subject to basespecific cleavage which depends on the presence of methylated cytosine in the original DNA sample. Cleavage products are then quantitatively analyzed by MALDI-TOF mass spectrometry. MALDI TOF MS analysis of the cleavage product results in a distinct signal pattern from the methylated and non-methylated template DNA. Individual methylation ratios for CpGs within a target sequence were determined and relative methylation ratios assessed in a range between 0%-100% methylation as indicated above each panel as a gradation of color change from yellow (0% methylation) to blue (100% methylation) with a standard deviation of 5%. Amplicon sizes are shown at the top of each data set (for example, JAG1 CTCF site 1 is approximately 225 bp). CpGs interrogated are successively numbered below the amplicon size bar (for example, JAG1 CTCF site 1 contains 7 CpGs of which methylation status was determinable for 5; CpGs 2-6). All amplicons were analyzed in duplicate as indicated (a and b). Control DNA was obtained from SV40 transformed lymphoblasts. Fully methylated DNA (*in vitro* enzymatically methylated genomic DNA) as well as fully unmethylated DNA (chemically and enzymatically treated genomic DNA) were also used as controls.

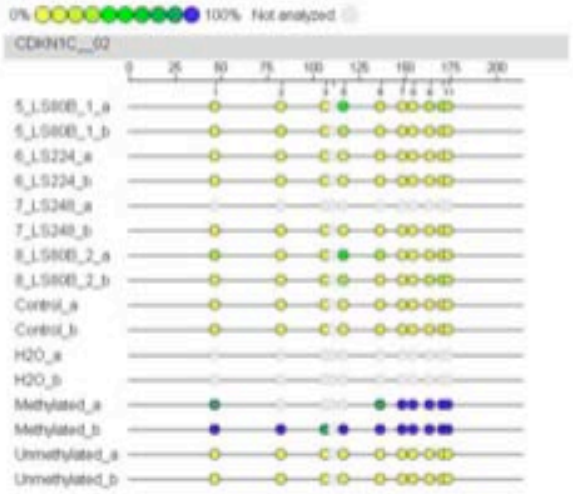
0% 100% Not analyzed
CDKN1C__02
5_LS80B_1_a
5_LS80B_1_b
6_LS224_a
6_LS224_b
7_LS248_a
7_LS248_b
8_LS80B_2_a
8_LS80B_2_b
Control_a
Control_b
H2O_a
H2O_b
Methylated_a
Methylated_b
Unmethylated_a
Unmethylated_b

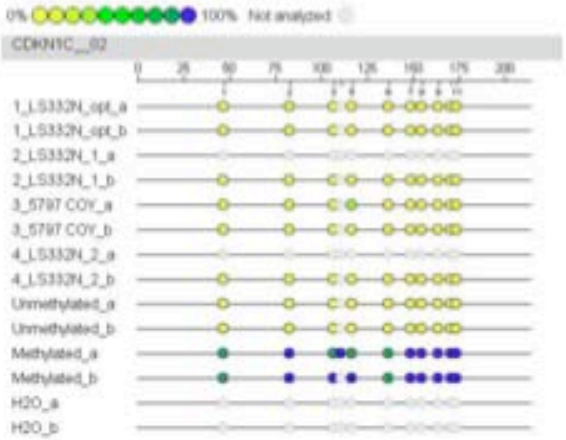
0% 100% Not analyzed
CDKN1C__02
1_LS332N_opt_a
1_LS332N_opt_b
2_LS332N_1_a
2_LS332N_1_b
3_5797 COY_a
3_5797 COY_b
4_LS332N_2_a
4_LS332N_2_b
Unmethylated_a
Unmethylated_b
Methylated_a
Methylated_b
H2O_a
H2O_b

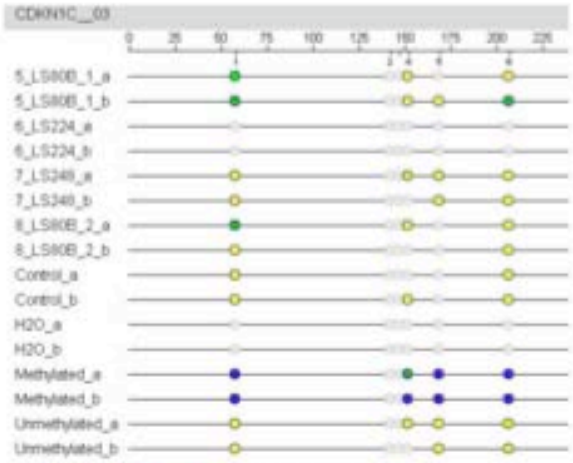
CDKN1C__03
5_LS80B_1_a
5_LS80B_1_b
6_LS224_a
6_LS224_b
7_LS248_a
7_LS248_b
8_LS80B_2_a
8_LS80B_2_b
Control_a
Control_b
H2O_a
H2O_b
Methylated_a
Methylated_b
Unmethylated_a
Unmethylated_b

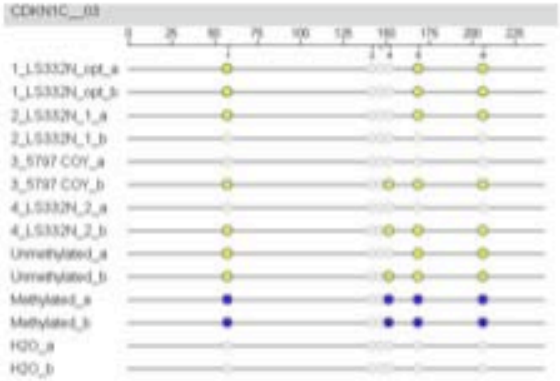
CDKN1C__03
1_LS332N_opt_a
1_LS332N_opt_b
2_LS332N_1_a
2_LS332N_1_b
3_5797 COY_a
3_5797 COY_b
4_LS332N_2_a
4_LS332N_2_b
Unmethylated_a
Unmethylated_b
Methylated_a
Methylated_b
H2O_a
H2O_b

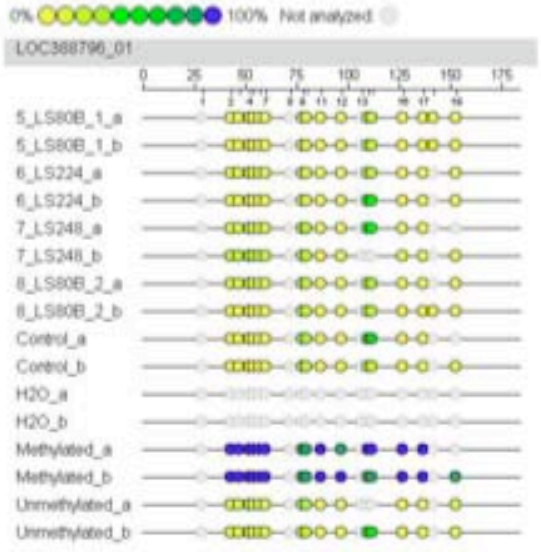
0% 100% Not analyzed
LOC388796_01
5_LS80B_1_a
5_LS80B_1_b
6_LS224_a
6_LS224_b
7_LS248_a
7_LS248_b
8_LS80B_2_a
8_LS80B_2_b
Control_a
Control_b
H2O_a
H2O_b
Methylated_a
Methylated_b
Unmethylated_a
Unmethylated_b

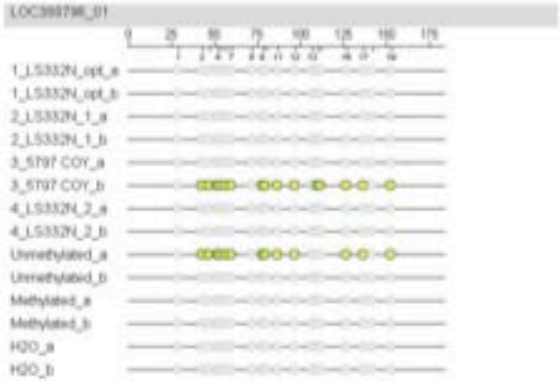
LOC388796_01
1_LS332N_opt_a
1_LS332N_opt_b
2_LS332N_1_a
2_LS332N_1_b
3_5797 COY_a
3_5797 COY_b
4_LS332N_2_a
4_LS332N_2_b
Unmethylated_a
Unmethylated_b
Methylated_a
Methylated_b
H2O_a
H2O_b

Figure 11: Quantitative DNA methylation analysis in ovarian cancers and normal ovarian epithelium for CTCF sites associated with CDNK1C and the 5'UTR of LOC388796. LCM captured DNA from three ovarian cancers (LS80B, LS224, and LS240) and two normal samples (LS332N and 5797 COY) was treated with sodium bisulfite. Converted DNAs were amplified with primers spanning CTCF binding sites or promoter regions for the indicated genes. PCR products were then subject to basespecific cleavage which depends on the presence of methylated cytosine in the original DNA sample. Cleavage products are then quantitatively analyzed by MALDI-TOF mass spectrometry. MALDI TOF MS analysis of the cleavage product results in a distinct signal pattern from the methylated and non-methylated template DNA. Individual methylation ratios for CpGs within a target sequence were determined and relative methylation ratios assessed in a range between 0%-100% methylation as indicated above each panel as a gradation of color change from yellow (0% methylation) to blue (100% methylation) with a standard deviation of 5%. Amplicon sizes are shown at the top of each data set (for example, CDNK1C CTCF site 2 is approximately 200 bp). CpGs interrogated are successively numbered below the amplicon size bar (for example, CDNK1C CTCF site 2 contains 11 CpGs of which methylation status was determinable for all but CpG 4). All amplicons were analyzed in duplicate as indicated (a and b). Control DNA was obtained from SV40 transformed lymphoblasts. Fully methylated DNA (*in vitro* enzymatically methylated genomic DNA) as well as fully unmethylated DNA (chemically and enzymatically treated genomic DNA) were also used as controls

NEOPLASIA
www.neoplasia.com

Volume 12 Number 12 December 2010 pp. 1–10 1

Identification of a Preneoplastic Gene Expression Profile in Tubal Epithelium of BRCA1 Mutation Carriers[1,2,3]

Joshua Z. Press*, Kaitlyn Wurz*,†, Barbara M. Norquist*, Ming K. Lee†, Christopher Pennil†, Rochelle Garcia‡, Piri Welcsh†, Barbara A. Goff* and Elizabeth M. Swisher*,†

*Division of Gynecologic Oncology, Department of Obstetrics and Gynecology, University of Washington School of Medicine, Seattle, WA, USA; †Division of Medical Genetics, Department of Medicine, University of Washington School of Medicine, Seattle, WA, USA; ‡Department of Pathology, University of Washington School of Medicine, Seattle, WA, USA

Abstract

Microinvasive carcinomas and high-grade intraepithelial neoplasms are commonly discovered within the fallopian tube of BRCA1 mutation carriers at the time of risk-reducing salpingo-oophorectomy, suggesting that many BRCA1-mutated ovarian carcinomas originate in tubal epithelium. We hypothesized that changes in gene expression profiles within the histologically normal fallopian tube epithelium of *BRCA1* mutation carriers would overlap with the expression profiles in *BRCA1*-mutated ovarian carcinomas and represent a *BRCA1* preneoplastic signature. Laser capture microdissection of frozen sections was used to isolate neoplastic cells or histologically normal fallopian tube epithelium, and expression profiles were generated on Affymetrix U133 Plus 2.0 gene expression arrays. Normal-risk controls were 11 women wild type for *BRCA1* and *BRCA2* (WT-FT). WT-FT were compared with histologically normal fallopian tube epithelium from seven women with deleterious *BRCA1* mutations who had foci of at least intraepithelial neoplasm within their fallopian tube (B1-FTocc). WT-FT samples were also compared with 12 *BRCA1* ovarian carcinomas (B1-CA). The comparison of WT-FT *versus* B1-FTocc resulted in 152 differentially expressed probe sets, and the comparison of WT-FT *versus* B1-CA resulted in 4079 differentially expressed probe sets. The BRCA1 preneoplastic signature was composed of the overlap between these two lists, which included 41 concordant probe sets. Genes in the *BRCA1* preneoplastic signature included several known tumor suppressor genes such as *CDKN1C* and *EFEMP1* and several thought to be important in invasion and metastasis such as *E2F3*. The expression of a subset of genes was validated with quantitative reverse transcription–polymerase chain reaction and immunohistochemistry.

Neoplasia (2010) 12, 1–10

Introduction

Ovarian carcinoma is the leading cause of death from gynecologic malignant neoplasms in the developed world. Identification of the early molecular events leading to ovarian carcinoma has been hindered by the lack of an identifiable preneoplastic lesion and the limited occurrence of early-stage neoplasms. Although it has been proposed that ovarian carcinoma originates from the surface epithelium of the ovary and/or the epithelial lining of ovarian inclusion cysts, there have been few reports of intraepithelial neoplasms at these sites [1,2].

Address all correspondence to: Joshua Z. Press, MD, Department of Obstetrics and Gynecology, University of Washington Medical Center, Box 356460, Seattle, WA 98195. E-mail: jzp@u.washington.edu

[1]This study was supported by the Yvonne Betson Trust, DOD OC073389 (to E.M.S.) and 1R01CA131965 (E.M.S.). No authors have conflicts of interest to declare.
[2]This study was presented in abstract form at the 40th Annual Society of Gynecologic Oncologists meeting in San Antonio, TX, 2009.
[3]This article refers to supplementary materials, which are designated by Tables W1 and W2 and Figures W1 to W4 and are available online at www.neoplasia.com.
Received 22 July 2010; Revised 6 September 2010; Accepted 9 September 2010

DOI 10.1593/neo.101044

Alternatively, there has been increasing evidence that many ovarian carcinomas originate within the fallopian tube [3]. Fallopian tube epithelium can exhibit areas of increased proliferation and cytologic atypia, called intraepithelial neoplasia (IEN). Most ovarian carcinomas are of serous histology and frequently exhibit mutations in the critical cell cycle regulator p53 [4]. Severe IEN in fallopian tubes has been found in conjunction with mullerian malignant neoplasms, particularly serous carcinomas of ovarian, uterine, or peritoneal origin [5,6]. Identical p53 mutations have been identified in tubal IEN and coexisting sporadic serous carcinoma [7], suggesting that genetic disruption within the fallopian tube may progress to ovarian carcinoma.

Further evidence for a tubal origin is suggested by the high prevalence of occult fallopian tube carcinomas identified among *BRCA1* and *BRCA2* mutation carriers undergoing risk-reducing salpingo-oophorectomy (RRSO). Although the lifetime risk of ovarian carcinoma in the general population is only 1% to 2%, women who inherit mutations in the *BRCA1* and *BRCA2* genes have up to a 50% lifetime risk of ovarian carcinoma [8]. These high-risk women are frequently discovered to have occult neoplasms at the time of RRSO, and 57% to 100% of these lesions arise in the fallopian tube [9–11]. Fallopian tube epithelium frequently contains areas that have been termed *p53 foci* (also referred to as p53 signatures), which overexpress p53 and have increased expression of the proliferation marker Ki-67 [12]. These tubal p53 foci are more frequent in tubes from BRCA1 and BRCA2 mutation carriers compared with normal-risk women, and they have also been shown to exhibit decreased expression of the tumor suppressor protein p27 [13]. These observations have resulted in the proposal of a new paradigm for ovarian carcinoma, in which the fallopian tube epithelium acquires a sequence of molecular abnormalities leading to an *in situ* or invasive neoplasm, which exfoliates and spreads to the ovary and peritoneum [3]. Validating the role of the fallopian tube in ovarian carcinoma carcinogenesis will require additional studies, such as comparative analysis of gene expression between wild-type and high-risk fallopian tubes.

We obtained frozen fallopian tube tissue from seven women with *BRCA1* mutations found to have occult invasive carcinomas or severe IEN in the fallopian tube on final pathologic examination. We hypothesized that the histologically normal tubal epithelium from these women would possess a gene expression profile that would reflect early alterations in gene expression contributing to the development of carcinoma. By comparing the gene expression profiles between these high-risk fallopian tubes and histologically normal fallopian tubes from women with wild-type *BRCA1* and *BRCA2*, we identified a set of genes potentially important in the development of *BRCA1*-associated carcinomas. We hypothesized that genes important in *BRCA1* ovarian carcinogenesis would have similarly altered expression patterns in *BRCA1* carcinomas. Therefore, we used the expression patterns in *BRCA1* ovarian carcinomas to further define the genes of interest in *BRCA1* tubal epithelium.

Materials and Methods

Study Design and Sample Selection

All tissues and clinical information were obtained from the University of Washington Gynecologic Oncology Tissue Bank according to an institutional review board–approved protocol. To maximize the likelihood of identifying biologically important gene differentially expressed between histologically normal BRCA wild-type fallopian tubes and high-risk fallopian tubes from *BRCA1* mutation carriers, we specifically selected *BRCA1* mutation carriers possessing occult microinvasive or high-grade intraepithelial fallopian tube neoplasm to create the gene profile (B1-FTocc). In addition, to minimize the false discovery rate, we also identified genes differentially expressed between the BRCA wild-type fallopian tube epithelium (WT-FT) and invasive *BRCA1* carcinomas (B1-CA). We limited our *BRCA1* preneoplastic profile to genes showing concordant up-regulation or down-regulation in both B1-FTocc and B1-CA. Thirty patients were analyzed to create the *BRCA1* preneoplastic gene signature: 11 histologically normal fallopian tube epithelium from women with wild-type *BRCA1* and *BRCA2* (WT-FT), 7 histologically normal fallopian tube epithelium from women with deleterious *BRCA1* mutations and documented occult microinvasive or high-grade intraepithelial fallopian tube carcinoma (B1-FTocc), and 12 high-grade serous ovarian carcinomas from women with deleterious *BRCA1* mutations (B1-CA). The characteristics of these patients are shown in Table 1. We chose WT-FT samples to match the age and menopausal distribution of the B1-FTocc cases. Some women in the WT-FT group had a personal history of breast cancer or a family history of breast cancer; however, women were excluded from the WT-FT group if they had a family history of ovarian cancer. All WT-FT control women had had full gene sequencing by Myriad genetics, and those who did not have comprehensive rearrangement testing performed by Myriad were screened with Multiplex Ligation–dependent Probe Amplification (MRC-Holland BV, Amsterdam, Holland) according to the manufacturer's instructions in our laboratory using normal DNA extracted from lymphocytes. For the B1-FTocc samples, the histologically normal epithelium was obtained from the same fallopian tube discovered to contain the occult fallopian tube neoplasm. Three of the seven B1-FTocc women were premenopausal at the time of oophorectomy.

Laser Capture Microdissection, RNA Amplification, and Gene Expression Chips

Tissues samples had been collected at the time of RRSO or ovarian carcinoma cytoreductive surgery and were immediately frozen in the operating room in liquid nitrogen in Tissue-Tek OCT (Alphen aan den Rijn, the Netherlands). For RRSO specimens, a small piece of tubal fimbriae was collected for the tissue bank. A frozen section of that tissue was stained with hematoxylin and eosin to confirm normal histologic diagnosis and rule out neoplasia in the research specimen. The remaining fallopian tube tissues from these cases were then subjected to serial sectioning by the pathologist to look for intraepithelial carcinoma or invasive carcinoma. All stored samples were subjected to the identical protocol of laser capture microdissection (LCM), linear RNA amplification, and microarray production. Hematoxylin and eosin slides from the frozen tissue OCT blocks were reviewed to select blocks with adequate distal fimbriated fallopian tube epithelium. Before LCM, 7-μm frozen sections were cut, adhered onto glass membrane slides (Arcturus, Mountain View, CA), and immediately stored on dry ice. Before LCM, the slides were dehydrated and stained with hematoxylin with the Histogene LCM Frozen Section Staining Kit (Arcturus). Slides were immediately transferred to the Veritas Laser Capture Microdissection system (Arcturus). Fallopian tube epithelium from the distal fimbriated fallopian tube was selectively captured for the fallopian tube samples, and ovarian carcinoma cells were selectively captured for neoplastic samples (Figure W1). Total RNA was isolated, and contaminating DNA was removed using the PicoPure RNA Isolation Kit (Arcturus) as per the company's protocol. The MessageAmp II aRNA amplification Kit (Ambion, Austin, TX) was used to amplify

Table 1. Cases Used to Generate the *BRCA1* Preneoplastic Gene Signature.

Case Identifier	Age (years)	Menopausal Status	*BRCA1/2* Status*	Other Characteristics
WT-FT no. 1	46	Pre	Negative	Personal history of breast cancer
WT-FT no. 2	47	Post	Negative	Personal history of breast cancer
WT-FT no. 3	48	Post	Negative	Personal history of breast cancer
WT-FT no. 4	48	Pre	Negative	No personal history of cancer
WT-FT no. 5	49	Post	Negative	Personal history of breast cancer
WT-FT no. 6	50	Pre	Negative	Personal history of breast cancer
WT-FT no. 7	52	Pre	Negative	Personal history of breast cancer
WT-FT no. 8	54	Post	Negative	Personal history of breast cancer
WT-FT no. 9	55	Post	Negative	Personal history of breast DCIS
WT-FT no. 10	61	Post	Negative	No personal history of cancer
WT-FT no. 11	61	Post	Negative	Personal history of breast cancer
B1-FTocc no. 1	39	Pre	B1.3109insAA	Microinvasion left fallopian tube
B1-FTocc no. 2	40	Post	B1.M1V (120A>G)	Microinvasion left fallopian tube
B1-FTocc no. 3	47	Pre	B1.2800delAA	High-grade intraepithelial
B1-FTocc no. 4	49	Pre	B1.3795del4	Microinvasion right fallopian tube†
B1-FTocc no. 5	53	Post	B1.del ex14-20	High-grade intraepithelial
B1-FTocc no. 6	62	Post	B1.C61G	High-grade intraepithelial
B1-FTocc no. 7	63	Post	B1.2800delAA	Microinvasion left fallopian tube
B1-CA no. 1	40	Pre	B1.2576.delC	Stage IIIC, grade 3, serous carcinoma
B1-CA no. 2	41	Pre	B1.185delAG	Stage IIIC, grade 3, serous carcinoma
B1-CA no. 3	44	Pre	B1.2798del4	Stage IIIC, grade 3, serous carcinoma
B1-CA no. 4	49	Pre	B1.3795del4	Stage IIIC, grade 3, serous carcinoma†
B1-CA no. 5	50	Post	B1.5382insC	Stage IA, grade 3, undifferentiated
B1-CA no. 6	51	Post	B1.3171ins5	Stage IIIC, grade 3, serous carcinoma
B1-CA no. 7	54	Post	B1.2594delC	Stage IV, grade 3, serous carcinoma
B1-CA no. 8	54	Post	B1.del_exon14	Stage IIIC, grade 3, serous carcinoma
B1-CA no. 9	55	Post	B1.M1V (120A>G)	Stage IIC, grade 3, serous carcinoma
B1-CA no. 10	57	Post	B1.5382insC	Stage IIIC, grade 3, mixed serous/endo
B1-CA no. 11	57	Post	B1.5382insC	Stage IIIC, grade 3, serous carcinoma
B1-CA no. 12	65	Post	B1.5382insC	Stage IIIC, grade 3, serous carcinoma

*Negative cases were wild-type by full sequencing as well as by comprehensive testing for gene rearrangements. WT-FT indicates histologically normal fallopian tube epithelium from *BRCA1* wild-type patients; B1-FTocc, histologically normal fallopian tube epithelium from patients with deleterious *BRCA1* mutations and at least high-grade intraepithelial fallopian tube neoplasm; B1-CA, tumor tissue from patients with deleterious *BRCA1* mutations.

†B1-FTocc no. 4 and B1-CA no. 4 are from the same individual who had both microscopic invasive neoplasm within the fallopian tube and peritoneal metastasis. DCIS indicates ductal carcinoma in situ. Menstrual phase of WT-FT cases: WT-FT no. 1 and WT-FT no. 7 had proliferative endometrium and WT-FT no. 4 and WT-FT no. 6 did not have hysterectomy performed.

the total RNA once. The quality of each amplified RNA sample was confirmed using Agilent 2000 Bioanalyzer RNA 6000 Pico LabChip Kit (Agilent Technologies, Inc, Santa Clara, CA), and quantity was measured using a NanoDrop ND-1000 Spectrophotometer (NanoDrop Technologies, Wilmington, DE). All labeling, hybridization, and scanning were performed at the University of Washington Centre for Array Technology core facility. Amplified complementary DNA (cDNA) was purified, enzymatically fragmented, and labeled with biotin. Quality and quantity of the purified labeled cDNA product were confirmed before hybridizing to Affymetrix GeneChip U133A Plus 2.0 Arrays (Affymetrix, Inc, Santa Clara, CA). To minimize batch effect, several samples from each study group were included in each batch of array runs.

Development of the Gene Expression Profile

GeneSifter (Seattle, WA) software was used for pairwise gene expression analysis and clustering analysis (Manhattan, Complete Linkage). For pairwise gene expression analysis, a Welch *t* test was used when generating *P* values. To develop a potential *BRCA1* preneoplastic gene expression profile, two independent comparisons were made. First, the 11 WT-FT were compared with the seven B1-FTocc samples, and probe sets were selected, which showed a 1.8-fold differential expression at $P < .01$. To minimize the false discovery rate, we also performed a comparison between the 11 WT-FT and 12 B1-CA and selected probe sets, which showed a 1.8-fold differential expression at $P < .01$. Probe sets were only selected for the *BRCA1* preneoplastic gene expression profile if they demonstrated concordant up-regulation or down-regulation in both the B1-FTocc and the B1-CA. The 1.8-fold was the cutoff at which we had most overlapping genes while still optimizing the ratio of overlapping genes to nonoverlapping genes.

Real-time Quantitative Reverse Transcription–Polymerase Chain Reaction Analysis

Real-time quantitative reverse transcription–polymerase chain reaction (RT-PCR) was used to validate the Affymetrix array results for four genes from the *BRCA1* preneoplastic signature. For each group (WT-FT, B1-FTocc, and B1-CA), five representative cases were selected and analyzed for expression of the four genes (*EFEMP1*, *p57*, *CYP3A5*, and *CSPG5*). TaqMan Gene Expression Assays (Applied Biosystems, Carlsbad, CA) were used for *EFEMP1* (Hs01013942_m1), *p57* (Hs00908986_g1), *CYP3A5* (Hs02511768_s1), and *CSPG5* (Hs00962721_m1), and *GAPDH* was used as the reference gene. All samples were run in triplicate, and the comparative C_t method was used for relative quantitation using ABI PRISM Sequence Detection Software (Applied Biosystems). Target gene C_t values were normalized to *GAPDH*.

Interrogation of the BRCA1 Preneoplastic Gene Signature Using Independent Samples

Additional fallopian tube samples that were not used to create the gene expression signature were selected to interrogate the *BRCA1* preneoplastic gene signature. To test the intrasample reproducibility of the tubal expression profiles, three duplicates of the B1-FTocc samples were analyzed (Table W1). For two of these B1-FTocc – DUP cases (B1-FTocc no. 2 – DUP and BT-FTocc no. 6 – DUP), expression arrays were created using tissue from the fallopian tube contralateral

to the microinvasive or high-grade intraepithelial lesion. For the duplicate of B1-FTocc no. 1, LCM was performed a second time using separate sections obtained approximately 100 μm further into the frozen tissue block. In addition, 12 *BRCA1*-mutated fallopian tubes from postmenopausal women, which did not contain occult lesions (B1-FT), were also analyzed (Table W2). The expression profiles were generated by comparing to the same set of WT-FT cases. These additional expression profiles were then analyzed by combining them one at a time with the original 30 samples that had been used to create the premaligant gene signature. Unsupervised hierarchical clustering (Manhattan, Complete Linkage) using the probe sets from the *BRCA1* preneoplastic gene signature was performed for each combination to determine whether the additional cases contained the *BRCA1* preneoplastic expression profile and would therefore cluster with the B1-FTocc cases. In addition, for 10 of the B1-CA carcinomas with adequate DNA available, DNA was sequenced for p53 exons 4 to 10 as previously described [14].

Ki-67 Immunohistochemistry

To validate the array gene expression data for *MKI67* (antigen identified by monoclonal antibody Ki-67), we performed immunohistochemistry on a larger set of fallopian tube samples, which had been stored as paraffin blocks. Most of these cases had right and left distal fallopian tube tissues available, and an average Ki-67 staining score was obtained from both tubes. Fallopian tube tissues from 26 *BRCA1* wild-type cases were compared with fallopian tube tissues from 52 *BRCA1* mutation carriers without carcinoma obtained at RRSO. Paraffin sections were deparaffinized and sequentially rehydrated, and endogenous peroxidases were blocked. Heat-mediated antigen retrieval was performed in a citrate buffer (Antigen Unmasking Solution; Vector Laboratories, Burlingame, CA). Slides were incubated with the Ki-67 mouse monoclonal antibody MIB-1, diluted 1:100 (Dako, Copenhagen, Denmark). Sections were washed with phosphate-buffered saline and incubated with secondary antibody (horseradish peroxidase–antimouse; Vector Laboratories). DAB was used to visualize antibody complexes, and sections were counterstained with hematoxylin. Negative and positive controls were assessed for each run. Slides were scored by two independent observers blinded to case designation. The percentages of positive epithelial cells were scored (0 = none, 1 = 1%, 2 = 2%-4%, 3 = 5%-15%, 4 ≥15%). A Mann-Whitney test was used to compare the staining results.

Results

Affymetrix Gene Expression

There were 18,600 probe sets expressed on the Affymetrix chips, which showed quality more than 0.7 in all samples. There were 152 probe sets with significant differential expression (>1.8-fold, $P < .01$) between the WT-FT and B1-FTocc. There were 4079 probe sets with significant differential expression (>1.8-fold, $P < .01$) between the WT-FT and B1-CA. The 152 probe sets differentially expressed from the BI-FTocc were compared with the 4079 differentially expressed probe sets in the B1-CA (Figure 1). The overlap between the two differentially expressed probe sets consisted of 29 probe sets downregulated in both groups, 12 probe sets upregulated in both groups, and 7 probe sets showing contradictory expression (up-regulation in one comparison and downregulated in the other). The 41 probe sets demonstrating concordant up-regulation or down-regulation in both comparisons comprised the *BRCA1* preneoplastic gene signature and are shown in Table 2 and Figure 2.

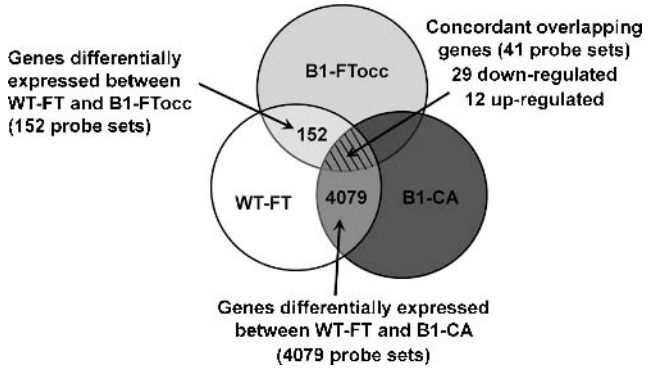

Figure 1. Diagram illustrating the protocol used to define the BRCA1 preneoplastic gene signature: Pairwise comparison between the WT-FT group and the B1-FTocc group (fold change ≥ 1.8, $P < .01$) identified 152 differentially expressed probe sets. Pairwise comparison between the WT-FT group and the B1-CA group (fold change ≥ 1.8, $P < .01$) identified 4079 differentially expressed probe sets. To minimize the false discovery rate, probe sets were only included in the gene signature with concordant down-regulation or up-regulation in both pairwise comparisons (hatched region).

To test the significance of the overlap in differentially expressed genes, we created a simulation in which there were 4079 randomly selected expressed clones in one group and 152 in a second group from 18,600 expressed clones and compared overlap. We repeated this simulation 10,000 times. A total of 21 overlapping clones were only observed in 1 (0.01%) of 10,000 simulations, and 22 or more overlapping genes were never observed. These data suggest that the overlap of 41 genes between our BRCA1 tubal epithelium and BRCA1 carcinomas is highly significant and that it did not occur by chance. The concordance of direction of the expression differences in 41 (85%) of 48 overlapping probes also suggests that overlap in differentially expressed genes is nonrandom.

Real-time Quantitative RT-PCR Analysis

Figure 3 shows the Affymetrix expression array results imposed beside the real-time quantitative RT-PCR results for each of the four selected genes (*EFEMP1*, *p57*, *CYP3A5*, and *CSPG5*). For each gene, the real-time quantitative RT-PCR shows a similar expression pattern to the corresponding Affymetrix array.

Clustering Analysis

The 30 samples used to create the *BRCA1* preneoplastic gene signature were subjected to unsupervised hierarchical clustering analysis using all 18,600 probe sets expressed with quality greater than 0.7 (Figure W2). The B1-CA formed a distinct group, but the clustering of the B1-FTocc and WT-FT did not generate any distinct pattern using all expressed probe sets. Interestingly, using only the 41 overlapping probes, the wild-type samples separated into distinct premenopausal and postmenopausal groups, which they did not do when clustering was based on the entire expressed probe set. Of 10 carcinomas evaluated, 6 contained a somatic p53 mutation determined by sequencing p53 exons 4 to 10 (data not shown). Carcinomas 2, 5, 6, 7, 10, and 11 had p53 mutations, whereas carcinomas 1, 3, 9, and 12 were wild-type. The p53 mutation status was not associated with how the carcinomas clustered when considering the 41 overlapping probe sets or all of the 18,600 expressed probes.

Table 2. The 41 Probe Sets Demonstrating Concordant Up-regulation or Down-regulation in Both Comparisons between WT-FT and B1-FTocc or B1-CA.

Affymetrix Probe Set	Gene Name	Gene Symbol	WT-FT *vs* B1-FTocc		WT-FT *vs* B1-CA	
			Fold	*P*	Fold	*P*
Downregulated						
230130_at	Transcribed locus	Unknown	3.7	.0020	3.4	.0054
214078_at	Primary neuroblastoma cDNA	Unknown	3.6	.0003	7.4	.0001
201843_s_at	EGF-containing fibulin-like extracellular matrix protein 1	*EFEMP1*	3.4	.0015	12.4	.0001
205568_at	Aquaporin 9	*AQP9*	2.7	.0021	3.4	.0020
214235_at	Cytochrome P450, family 3, subfamily A	*CYP3A5*	2.7	.0048	5.2	.0023
226228_at	Aquaporin 4	*AQP4*	2.6	.0081	7.7	.0003
213182_x_at	Cyclin-dependent kinase inhibitor 1C (p57, Kip2)	*CDKN1C*	2.5	.0008	3.1	.0014
203710_at	Inositol 1,4,5-triphosphate receptor, type 1	*ITPR1*	2.4	.0004	3.7	.0002
214607_at	p21 (CDKN1A)-activated kinase 3	*PAK3*	2.4	.0070	5.8	.0002
231183_s_at	Jagged 1 (Alagille syndrome)	*JAG1*	2.3	.0002	1.9	.0011
218656_s_at	Lipoma HMGIC fusion partner	*LHFP*	2.3	.0032	2.8	.0083
218717_s_at	Leprecan-like 1	*LEPREL1*	2.3	.0034	2.9	.0034
229480_at	MRNA; cDNA DKFZp686I18116	Unknown	2.1	.0018	2.2	.0002
209506_s_at	Nuclear receptor subfamily 2, group F, member 1	*NR2F1*	2.1	.0036	7.5	.0000
231262_at	Transcribed locus	Unknown	2.1	.0035	3.0	.0088
201497_x_at	Myosin, heavy chain 11, smooth muscle	*MYH11*	2.1	.0068	15.5	.0000
236277_at	Primary neuroblastoma cDNA	Unknown	2.0	.0094	3.5	.0001
201885_s_at	Cytochrome b5 reductase 3	*CYB5R3*	2.0	.0004	1.8	.0066
230233_at	Transcribed locus	Unknown	2.0	.0047	1.9	.0073
1557866_at	Chromosome 9 open reading frame 117	*C9orf117*	2.0	.0013	6.0	.0001
201162_at	Insulin-like growth factor binding protein 7	*IGFBP7*	2.0	.0088	6.1	.0000
201427_s_at	Selenoprotein P, plasma, 1	*SEPP1*	2.0	.0004	2.3	.0010
213451_x_at	Transcribed locus, sim to tenascin XB isoform 1	*TNXB*	1.9	.0072	5.3	.0002
218087_s_at	Sorbin and SH3 domain containing 1	*SORBS1*	1.9	.0082	2.1	.0038
204235_s_at	GULP, engulfment adaptor PTB domain containing 1	*GULP1*	1.9	.0006	4.8	.0000
218718_at	Platelet-derived growth factor C	*PDGFC*	1.9	.0007	1.8	.0059
209575_at	Interleukin 10 receptor, beta	*IL10RB*	1.9	.0010	1.8	.0016
209505_at	Nuclear receptor subfamily 2, group F, member 1	*NR2F1*	1.8	.0096	7.0	.0000
37005_at	Neuroblastoma, suppression of tumorigenicity 1	*NBL1*	1.8	.0066	2.5	.0017
Upregulated						
225857_s_at	Hypothetical LOC388796	*LOC388796*	2.4	.0000	2.6	.0000
238482_at	Kruppel-like factor 7 (ubiquitous)	*KLF7*	2.4	.0020	2.2	.0050
39966_at	Chondroitin sulfate proteoglycan 5	*CSPG5*	2.1	.0030	6.2	.0000
203693_s_at	E2F transcription factor 3	*E2F3*	2.1	.0054	6.4	.0000
1560622_at	CDNA FLJ20196 fis, clone COLF0944	Unknown	2.0	.0038	2.2	.0005
201577_at	Nonmetastatic cells 1, protein (NM23A)	*NME1*	1.9	.0066	3.0	.0002
65588_at	Hypothetical LOC388796	*LOC388796*	1.9	.0000	2.3	.0001
224474_x_at	SMEK homolog 2, suppressor of mek1	*SMEK2*	1.9	.0087	2.0	.0037
212020_s_at	Antigen identified by monoclonal antibody Ki-67	*MKI67*	1.9	.0056	3.5	.0000
224623_at	Transcribed locus, similar THO complex 3	*THOC3*	1.8	.0003	3.2	.0000
1560258_a_at	*Homo sapiens*, clone IMAGE:5590287, mRNA	Unknown	1.8	.0044	3.0	.0000
216262_s_at	TGFB-induced factor homeobox 2	*TGIF2*	1.8	.0094	1.8	.0033

The duplicated samples from the B1-FTocc group were then added to the clustering analysis and subjected to unsupervised hierarchical clustering using the BRCA1 preneoplastic gene signature. As shown in Figure W3, each of the duplicated samples clustered closely with their paired sample even when obtained from the contralateral FT, demonstrating the reproducibility of the expression profile in independent experiments as well as the consistency between paired bilateral fallopian tubes.

To further interrogate the *BRCA1* preneoplastic gene signature, expression profiles from 12 additional B1-FT that had not been used in developing the expression profile were each individually combined with the 30 samples used to create the signature and subjected to unsupervised hierarchical clustering using the *BRCA1* preneoplastic gene signature. Five of the new samples clustered with the B1-FTocc/B1-CA group, whereas seven of the new samples clustered with the WT-FT (Table W2). A representative example of each clustering pattern is shown in Figure W4. This suggested that 5 (42%) of the 12 B1-FT had experienced sufficient molecular disruptions to resemble B1-FTocc or B1-CA samples. Although the remaining seven B1-FT test samples clustered with wild-type fallopian tubes, they always clustered with the group from premenopausal women.

Ki-67 Immunohistochemistry

The Affymetrix array analysis showed a significantly increased expression of *MKI67* (gene for the antigen identified by monoclonal antibody Ki-67) in the B1-FTocc compared with WT-FT ($P = .01$; Figure 4*A*). To confirm the generalizability of the preneoplastic expression pattern in a larger set of wild-type and *BRCA1* histologically normal FT, we evaluated Ki-67 protein expression by immunohistochemistry in a larger set of paraffin-embedded FT specimens. Significantly higher Ki-67 protein expression was identified in fallopian tubes from *BRCA1* mutation carriers than from *BRCA1* wild-type women ($P = .0002$) who did not have cancer (Figure 4*B*). Representative images of low Ki-67 staining in WT-FT (Figure 4*C*) and high Ki-67 staining in B1-FT (Figure 4*D*) are shown.

Discussion

For many years, it was believed that ovarian carcinoma arises from the ovarian surface epithelium or in cortical inclusion cysts in the ovary. In accordance with this belief, most studies assessing disruption of gene expression in ovarian carcinomas have focused on the ovarian surface epithelium and carcinomas within the ovarian tissue [15]. However,

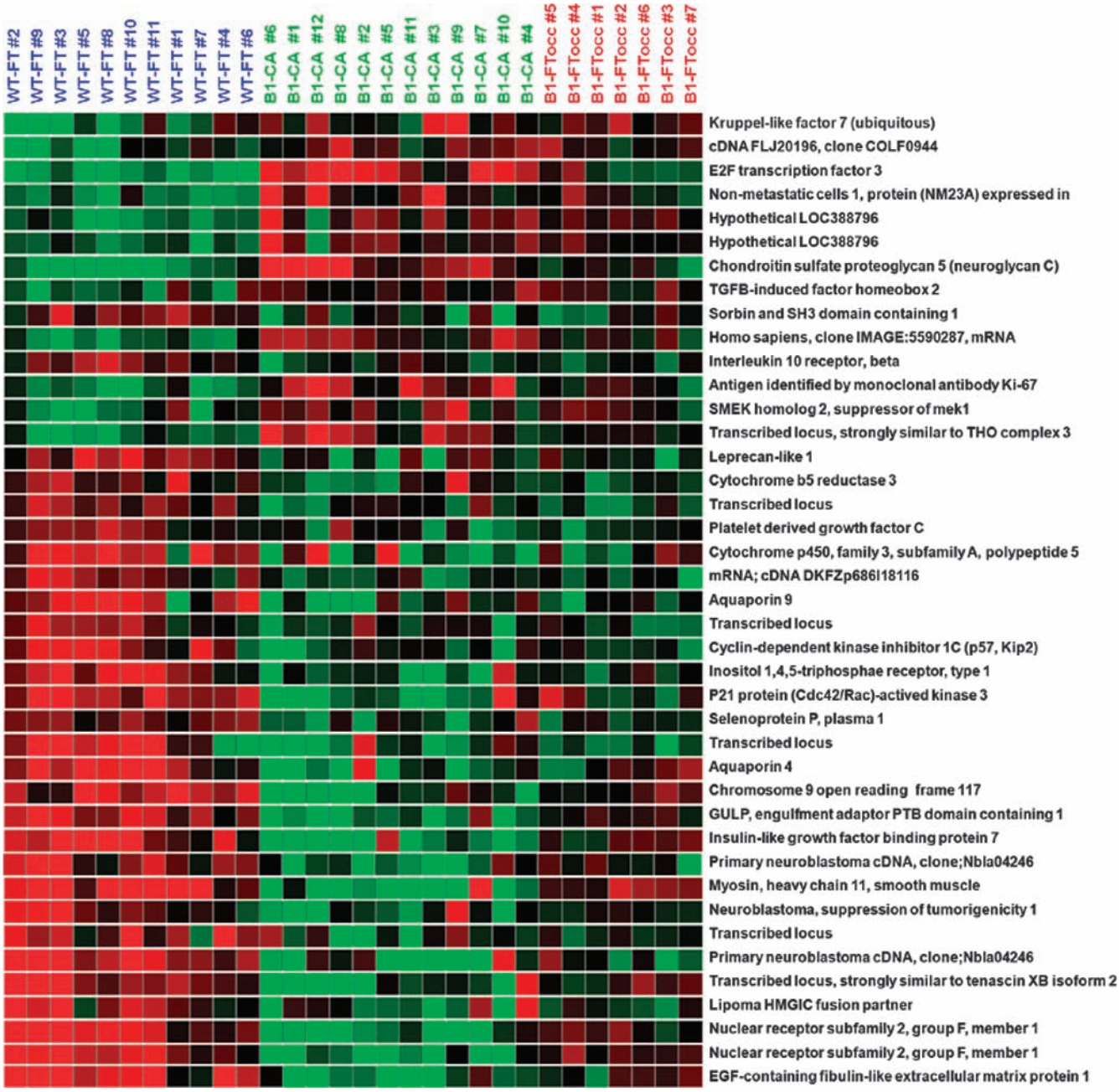

Figure 2. The 41 probe sets in the *BRCA1* preneoplastic profile include several known tumor suppressors and oncogenes.

the relevance of the ovarian surface epithelium has come under increasing scrutiny, and a comprehensive review of the literature regarding the origin of ovarian carcinoma concluded that there is insufficient evidence to support ovarian surface epithelium or inclusion glands as the origin of ovarian carcinomas [16]. In contrast, there has been increasing evidence that many ovarian and primary peritoneal carcinomas arise from neoplastic alterations within the fallopian tube epithelium. This view has been supported by the frequent discovery of occult fallopian tube neoplasms in fallopian tubes removed prophylactically from women at high risk due to hereditary *BRCA1* or *BRCA2* mutations [9–11]. The tubal epithelium in women with *BRCA1* mutations who have up to a 50% lifetime risk of ovarian carcinoma could represent a unique opportunity to study at-risk tissues just before neoplastic transformation. We hypothesized that the epithelium in these high-risk fallopian tubes would express some of the earliest gene disruptions leading to ovarian carcinoma.

Half of all *BRCA1* mutation carriers never develop ovarian carcinoma. This fact could make it difficult to identify a *BRCA1* preneoplastic gene expression profile in normal BRCA1 tubal epithelium in cancer-free *BRCA1* mutation carriers. Our current study is unique because we used histologically normal fallopian tube epithelium from the same fallopian tubes that contained at least a high-grade intraepithelial neoplasm. By using tissues already proven susceptible to neoplastic transformation, we improved our ability to identify a *BRCA1* preneoplastic expression profile in *BRCA1* mutation carriers. We predicted that gene expression differences that precede morphologically identifiable neoplastic transformation should also be present in *BRCA1*-associated ovarian carcinomas. Indeed, 41 of 152 differentially expressed probe sets in

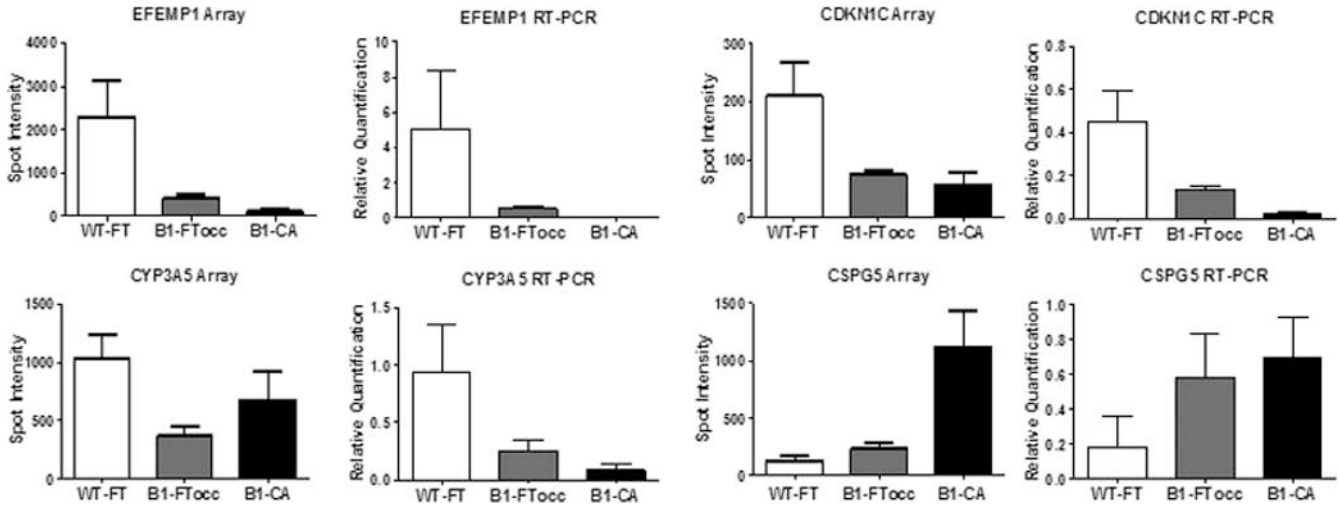

Figure 3. Correlation between expression array and real-time quantitative RT-PCR results: Four genes from the gene signature were selected for validation by RT-PCR with TaqMan assays. Five cases were used from each group (WT-FT, B1-FTocc, and B1-CA). The four genes included *EFEMP1* (EGF-containing fibulin-like extracellular matrix protein 1), *CDKN1C* (cyclin-dependent kinase inhibitor 1C or p57), *CYP3A5* (cytochrome P450, family 3, subfamily A), and *CSPG5* (chondroitin sulfate proteoglycan 5 or neuroglycan C). For each gene, the array expression data are shown beside the corresponding RT-PCR results.

the normal tubal epithelium from *BRCA1* mutation carriers with tubal neoplasia were also similarly differentially expressed in the *BRCA1* carcinomas when compared with tubal epithelium from normal-risk women. Our computer model confirmed that the identified overlap in expression profiles between *BRCA1* tubal epithelium and *BRCA1* carcinoma is highly significant, suggesting that the expression profile that we termed the *BRCA1 preneoplastic signature* represents a true biological phenomenon. The 41 overlapping probe sets represent unique genes altered in

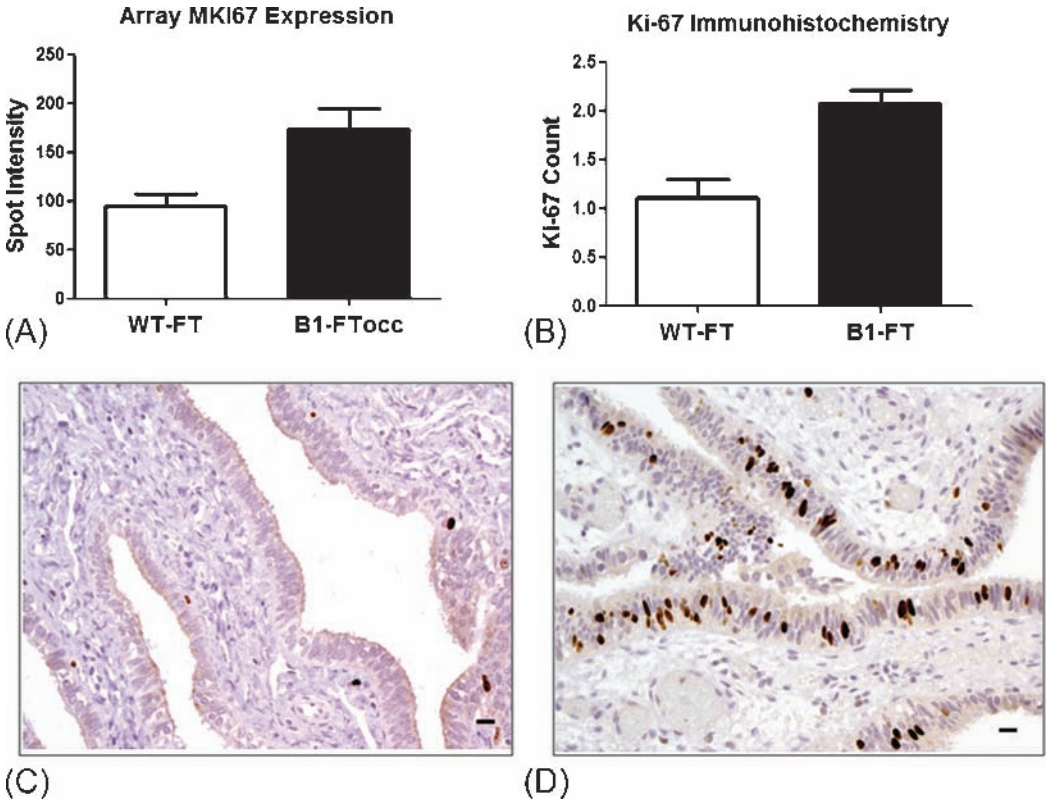

Figure 4. Validation of *MIK67* expression data with Ki-67 immunohistochemistry in 26 WT-FT and 52 B1-FT. (A) *MIK67* gene expression in the 11 WT-FT samples compared with the 7 B1-FTocc samples ($P = .01$). (B) Ki-67 protein expression (brown) in the fallopian tubes from 26 wild-type women compared with fallopian tubes from 52 women with deleterious *BRCA1* mutations ($P = .0002$). Representative images of low Ki-67 expression in a wild-type case (C) and high Ki-67 staining in a *BRCA1*-mutated case (D).

progression from normal fallopian tube epithelium to carcinoma. Furthermore, many of these 41 probe sets represent genes that have been shown to play an important role in cancer biology, such as *EFEMP1*, *CYP3A5*, *CDKN1C*, *NR2F1*, *E2F3*, *MKI67*, *NME1*, and *CSPG5*.

One gene in the *BRCA1* preneoplastic signature overexpressed in BRCA1 FT is the gene encoding the Ki-67 antigen, expressed in the nuclei of proliferating cells. To generalize our findings to other cases from women with known *BRCA1* mutations, we performed immunohistochemistry in a larger series of normal FTs. Consistent with the array data, our pathologists (who were blinded to case designation) identified significantly higher Ki-67 protein expression in FT epithelium of women with *BRCA1* mutations compared to women with negative genetic testing (Figure 4). These data suggest that at least some elements of the *BRCA1* preneoplastic signature are generalizable to BRCA1-mutated FTs without neoplasia. These data suggest that before neoplastic transformation, there exists a higher rate of proliferation in *BRCA1* tubal epithelium, which could increase the opportunity for somatic clonal genetic changes (such as loss of the wild-type allele) and subsequent neoplastic development.

Examples of downregulated probe sets in the *BRCA1* preneoplastic signature include those representing *EFEMP1*, *CDKN1C*, and *NR2F1*. Decreased expression of each of these genes has been implicated in carcinogenesis in a variety of neoplasms. *EFEMP1* (FLBN3) is a member of the fibulin family, a family of secreted glycoproteins with repeated epidermal growth factor domains and a unique C-terminal fibulin-type module. Fibulins mediate cell-to-cell and cell-to-matrix communication within the extracellular matrix [17]. Mutations in *EFEMP1* cause an autosomal-dominant disorder associated with early onset macular degeneration (Doyne honeycomb retinal dystrophy), which has been associated with excessive angiogenesis [18]. *EFEMP1* has antiangiogenic properties and has been shown to inhibit tumor growth in mice. The expression of *EFEMP1* is reduced in many human neoplasms, including ovarian carcinoma [19], and *EFEMP1* is inactivated by promoter methylation in 38% of primary lung carcinomas but not in paired normal lung tissue [20]. The cell cycle regulatory gene *CDKN1C* (p57/Kip2) is an imprinted maternally expressed gene on chromosome 11p15.4. Disruption of *CDKN1C* expression causes the cancer predisposing Beckwith-Wiedemann syndrome [21]. *CDKN1C* has also been implicated as a tumor suppressor gene in a number of human malignant neoplasms including breast, lung, pancreatic, bladder, esophageal, and a variety of hematological and myeloid neoplasms [22,23]. Prostate explants from a *CDKN1C* knockout mouse develop IEN and prostate adenocarcinoma in nude mice, providing the first mouse model that is pathologically identical to human prostate carcinoma [24]. *CDKN1C* dysregulation has not been extensively studied in ovarian carcinoma, but the majority (75%) of sporadic ovarian carcinomas demonstrate reduced CDKN1C protein expression (<10% of tumor cells) using immunohistochemistry [25]. *NR2F1* encodes for the protein chicken ovalbumin upstream promoter transcription factor I (COUP-TF1). COUP-TF1 is a nuclear receptor that has been shown to repress transcription, influence the tumor necrosis factor α signaling pathway [26], and modulate the retinoic acid receptor [27]. In breast carcinoma, decreased expression of COUP-TF1 is associated with the up-regulation of aromatase expression [28]. Decreased expression of COUP-TF1 has also been observed in ovarian and bladder carcinomas [29,30].

Upregulated probe sets in our *BRCA1* preneoplastic signature included *E2F3*, *NME1*, *CSPG5*, and *MKI67*. The *E2F3* gene is a transcription factor that has been implicated in malignant transformation of human lung [31], prostate [32], and bladder carcinomas [33]. Up-regulation of E2F transcription factors has been shown to influence disruptions of the cell cycle in high-grade serous ovarian carcinomas [34], and E2F3 has been used as a biomarker for ovarian carcinoma [35]. The E2F3–Aurora-A axis has been implicated in colorectal cancer [36] and ovarian cancer [37], and recently, *E2F3* has been implicated in the proliferation of ovarian cancer cells through interaction with epidermal growth factor receptor [38]. *NME1* (*NM23*) overexpression has been associated with decreased overall survival in patients with serous ovarian carcinoma [39]. *CSPG5* (neuroglycan C, neuregulin-6) is a growth factor that transactivates the *ErbB2* (HER2/*neu*) oncogene. *CSPG5* is a membrane-anchored chondroitin sulfate proteoglycan that stimulates cell proliferation in a dose-dependent fashion, acts as a specific ligand for ErbB3, and is capable of transactivation of ErbB2 (HER2) [40]. *ErbB2* (HER2/*neu*) is a well-recognized oncogene capable of inducing cellular proliferation and disrupting epithelial cellular polarity. Although *CSPG5* has not been well studied in human malignant neoplasms, *CSPG5* is secreted by neural stem cells, and it promotes its own proliferation in the fetal brain [41].

The traditional clonal model of carcinogenesis states that clonal expansion and neoplastic proliferation stem from genetic disruptions within an individual cell. However, a more contemporary hypothesis called the *epigenetic progenitor model* proposes that before this clonal event, there are global epigenetic alterations in nonneoplastic cell lines that allow the proliferation of cell line–specific stem or progenitor cells. This results in a large population of epigenetically disrupted progenitor cells that could then be affected by an initiating mutation of a key gatekeeper gene in a single cell [42]. An epigenetic progenitor model could explain our ability to identify global alterations of gene expression of key tumor progenitor genes in at-risk epithelium in areas that do not have histologically identifiable neoplastic proliferation. Further epigenetic studies will be necessary to assess this hypothesis in *BRCA1* tubal epithelium.

We assessed whether the tubal expression profile was consistent between various areas of the distal FT by performing unsupervised hierarchical clustering using independent samples from three of the B1-FTocc cases (two from the contralateral tube). Regardless of whether the duplicated samples were created from the ipsilateral or contralateral fallopian tube, all three duplicates clustered immediately adjacent to their corresponding sample when considering the preneoplastic gene signature (Figure W3). This suggests that the gene disruptions we observed in high-risk fallopian tubes represent a global field effect that affects bilateral fallopian tubes in patients with *BRCA1* mutations.

p53-immunopositive foci have been frequently observed in tubal epithelium of both high-risk and normal-risk women [3,13]. We made no effort to select p53-positive cells to derive the BRCA1 preneoplastic expression profile. The resulting expression profile did not seem to be driven by p53 because the expression profiles from the p53 wild-type carcinomas were not distinct from the p53 mutant carcinomas when just considering these genes. The probe sets on the Affymetrix array representing p53 showed minimal signal regardless of BRCA1 status. This is not surprising because p53 foci are generally small, occurring in as few as 10 cells and, consequently, would only be present in a small fraction of the cells that we used for expression array analysis. p53 foci likely represent a clonal event (somatic mutation) in a small subset of tubal epithelial cells. The fact that we can detect differences in expression profiles of *BRCA1* tubal epithelium despite not selecting for p53 foci implies that global alterations in gene expression including *MKI67* (Ki-67 protein) occur even in cells that do not have p53 alterations or mutation. These data support an alternate model in which

global alterations (including increased Ki-67) precede somatic clonal events such as p53 mutation in p53 foci [13].

Three of the seven B1-FTocc samples available from our tissue bank were collected from premenopausal women. To equalize the menopausal status in our three groups, we specifically included cases in the WT-FT and B1-CA groups that were premenopausal at the time of surgery. When unsupervised hierarchical clustering was performed using the preneoplastic gene signature, the four premenopausal WT-FT cases formed a distinct group from the seven postmenopausal WT-FT cases. Interestingly, when the 12 additional FT-B1 samples (which were all postmenopausal) were subjected to clustering analysis, the 7 samples that clustered with the WT-FT group always clustered with the premenopausal WT-FT. It seems that BRCA1-mutated fallopian tubes maintain a gene expression profile that is more similar to premenopausal tissue, even without the stimulation of the premenopausal hormonal milieu. Our group has recently demonstrated that proliferation in WT-FT as measured by Ki-67 protein expression decreases with age, but Ki-67 expression is maintained at a higher level with a less marked decrease with age in women with *BRCA1* mutation [13]. Therefore, both protein expression and expression profiling suggest that *BRCA1* fallopian tube epithelium maintains a premenopausal proliferative phenotype. Overall, 5 (42%) of the 12 additional B1-FT samples clustered with the B1-FTocc/B1-CA group based on the *BRCA1* preneoplastic signature. This closely reflects the percentage of women with *BRCA1* mutations who will go on to develop ovarian carcinoma [8]. Interestingly, the samples that clustered with the B1-FTocc/B1-CA group had higher Ki-67 staining.

There has only been one published study by Tone et al. [43] looking at differential gene expression profiles from *BRCA1*-mutated fallopian tube epithelium and fallopian tube/ovarian carcinomas, which was designed differently from our study. These investigators analyzed fallopian tube epithelium only from premenopausal women, included both *BRCA1* and *BRCA2* mutation carriers, and focused on fallopian tubes without associated carcinoma, as opposed to our strategy of microdissecting epithelium from fallopian tubes containing at least high-grade intraepithelial neoplasm. Furthermore, their carcinoma group included sporadic fallopian tube and ovarian carcinomas, whereas we compared expression profiles specifically to BRCA1-mutated carcinomas. We felt it was important to separate BRCA1 from BRCA2 fallopian tube epithelium given that ovarian carcinomas have distinct different expression profiles according to whether they have a *BRCA1* or *BRCA2* mutation [44]. They observed that *BRCA1*-mutated fallopian tubes collected during the luteal phase of the menstrual cycle were more likely to cluster with the carcinoma samples. They hypothesized that the hormonal environment of the luteal phase causes distinct changes in high-risk fallopian tubes resulting in similar gene expression to carcinoma tissue. Because of the different approaches between this study and our current study, it is difficult to compare the specific genes identified. However, both studies suggest that fallopian tube epithelium from *BRCA1* mutation carriers is susceptible to disruption in gene expression, which causes histologically normal fallopian tube tissue to exhibit gene expression resembling carcinoma.

By analyzing gene expression from histologically normal fallopian tube epithelium isolated from *BRCA1*-mutated fallopian tubes containing early neoplasms, we have identified a potential *BRCA1* preneoplastic gene expression signature for *BRCA1* serous carcinoma. This gene signature may include some of the earliest disruptions in gene expression leading to the development of serous ovarian carcinoma. Further validation will be necessary to determine which of the genes from this signature are critical in this process and to identify the mechanisms of gene expression alterations. The fact that these genes are disrupted in the fallopian tube tissue before the development of invasive carcinoma could make them useful targets for chemoprevention or early detection of ovarian carcinoma.

Acknowledgments

The authors thank Mary-Claire King for her support and guidance in this project, the staff at the Centre for Array Technology for their assistance with processing gene expression arrays, Danbin Xu for guidance with real-time PCR analysis, Robert Vessella and Colm Morrissey for assistance with LCM, Lawrence True for guidance with tissue preparation, and Peter Nelson and Ilsa Coleman for LCM and expression array protocols.

References

[1] Cai KQ, Klein-Szanto A, Karthik D, Edelson M, Daly MB, Ozols RF, Lynch HT, Godwin AK, and Xu XX (2006). Age-dependent morphological alterations of human ovaries from populations with and without *BRCA* mutations. *Gynecol Oncol* **103**, 719–728.

[2] Schlosshauer PW, Cohen CJ, Penault-Llorca F, Miranda CR, Bignon YJ, Dauplat J, and Deligdisch L (2003). Prophylactic oophorectomy: a morphologic and immunohistochemical study. *Cancer* **98**, 2599–2606.

[3] Crum CP, Drapkin R, Miron A, Ince TA, Muto M, Kindelberger DW, and Lee Y (2007). The distal fallopian tube: a new model for pelvic serous carcinogenesis. *Curr Opin Obstet Gynecol* **19**, 3–9.

[4] Kmet LM, Cook LS, and Magliocco A (2003). A review of p53 expression and mutation in human benign, low malignant potential, and invasive epithelial ovarian tumors. *Cancer* **97**, 389–404.

[5] Stern J, Buscema J, Parmley T, Woodruff JD, and Rosenshein NB (1981). Atypical epithelial proliferations in the fallopian tube. *Am J Obstet Gynecol* **140**, 309–312.

[6] Yanai-Inbar I and Silverberg SG (2000). Mucosal epithelial proliferation of the fallopian tube: prevalence, clinical associations, and optimal strategy for histopathologic assessment. *Int J Gynecol Pathol* **19**, 139–144.

[7] Kindelberger DW, Lee Y, Miron A, Hirsch MS, Feltmate C, Medeiros F, Callahan MJ, Garner EO, Gordon RW, Birch C, et al. (2007). Intraepithelial carcinoma of the fimbria and pelvic serous carcinoma: evidence for a causal relationship. *Am J Surg Pathol* **31**, 161–169.

[8] King MC, Marks JH, and Mandell JB (2003). Breast and ovarian cancer risk due to inherited mutations in *BRCA1* and *BRCA2*. *Science* **302**, 643–646.

[9] Finch A, Shaw P, Rosen B, Murphy J, Narod SA, and Colgan TJ (2006). Clinical and pathologic findings of prophylactic salpingo-oophorectomies in 159 *BRCA1* and *BRCA2* carriers. *Gynecol Oncol* **100**, 58–64.

[10] Lamb JD, Garcia RL, Goff BA, Paley PJ, and Swisher EM (2006). Predictors of occult neoplasia in women undergoing risk-reducing salpingo-oophorectomy. *Am J Obstet Gynecol* **194**, 1702–1709.

[11] Leeper K, Garcia R, Swisher E, Goff B, Greer B, and Paley P (2002). Pathologic findings in prophylactic oophorectomy specimens in high-risk women. *Gynecol Oncol* **87**, 52–56.

[12] Lee Y, Miron A, Drapkin R, Nucci MR, Medeiros F, Saleemuddin A, Garber J, Birch C, Mou H, Gordon RW, et al. (2007). A candidate precursor to serous carcinoma that originates in the distal fallopian tube. *J Pathol* **211**, 26–35.

[13] Norquist BM, Garcia RL, Allison KH, Jokinen CH, Kernochan LE, Pizzi CC, Barrow BJ, Goff BA, and Swisher EM (in press). The molecular pathogenesis of hereditary ovarian carcinoma: alterations in the tubal epithelium of women with *BRCA1* and *BRCA2* mutations. *Cancer*.

[14] Galic V, Willner J, Wollan M, Garg R, Garcia R, Goff BA, Gray HJ, and Swisher EM (2007). Common polymorphisms in TP53 and MDM2 and the relationship to TP53 mutations and clinical outcomes in women with ovarian and peritoneal carcinomas. *Genes Chromosomes Cancer* **46**, 239–247.

[15] Fehrmann RS, Li XY, van der Zee AG, de Jong S, Te Meerman GJ, de Vries EG, and Crijns AP (2007). Profiling studies in ovarian cancer: a review. *Oncologist* **12**, 960–966.

[16] Bell DA (2005). Origins and molecular pathology of ovarian cancer. *Mod Pathol* **18**(suppl 2), S19–S32.

[17] Gallagher WM, Currid CA, and Whelan LC (2005). Fibulins and cancer: friend or foe? *Trends Mol Med* **11**, 336–340.

[18] Stone EM, Lotery AJ, Munier FL, Héon E, Piguet B, Guymer RH, Vandenburgh K, Cousin P, Nishimura D, Swiderski RE, et al. (1999). A single *EFEMP1* mutation associated with both Malattia Leventinese and Doyne honeycomb retinal dystrophy. *Nat Genet* **22**, 199–202.

[19] Albig AR, Neil JR, and Schiemann WP (2006). Fibulins 3 and 5 antagonize tumor angiogenesis *in vivo*. *Cancer Res* **66**, 2621–2629.

[20] Yue W, Dacic S, Sun Q, Landreneau R, Guo M, Zhou W, Siegfried JM, Yu J, and Zhang L (2007). Frequent inactivation of *RAMP2*, *EFEMP1* and *Dutt1* in lung cancer by promoter hypermethylation. *Clin Cancer Res* **13**, 4336–4344.

[21] Hatada I, Ohashi H, Fukushima Y, Kaneko Y, Inoue M, Komoto Y, Okada A, Ohishi S, Nabetani A, Morisaki H, et al. (1996). An imprinted gene $p57^{KIP2}$ is mutated in Beckwith-Wiedemann syndrome. *Nat Genet* **14**, 171–173.

[22] Larson PS, Schlechter BL, King CL, Yang Q, Glass CN, Mack C, Pistey R, de Las Morenas A, and Rosenberg CL (2008). *CDKN1C/*$p57^{kip2}$ is a candidate tumor suppressor gene in human breast cancer. *BMC Cancer* **8**, 68.

[23] Kikuchi T, Toyota M, Itoh F, Suzuki H, Obata T, Yamamoto H, Kakiuchi H, Kusano M, Issa JP, Tokino T, et al. (2002). Inactivation of $p57^{KIP2}$ by regional promoter hypermethylation and histone deacetylation in human tumors. *Oncogene* **21**, 2741–2749.

[24] Jin RJ, Lho Y, Wang Y, Ao M, Revelo MP, Hayward SW, Wills ML, Logan SK, Zhang P, and Matusik RJ (2008). Down-regulation of $p57^{Kip2}$ induces prostate cancer in the mouse. *Cancer Res* **68**, 3601–3608.

[25] Khouja MH, Baekelandt M, Nesland JM, and Holm R (2007). The clinical importance of Ki-67, p16, p14, and p57 expression in patients with advanced ovarian carcinoma. *Int J Gynecol Pathol* **26**, 418–425.

[26] Zhang LJ, Liu X, Gafken PR, Kioussi C, and Leid M (2008). A chicken ovalbumin upstream transcription factor 1 (COUP-TF1) complex represses expression of the gene encoding tumor necrosis factor α–induced protein 8 (*TNFAIP8*). *J Biol Chem* **284**, 6156–6168.

[27] Lin B, Chen GQ, Xiao D, Kolluri SK, Cao X, Su H, and Zhang XK (2000). Orphan receptor COUP-TF is required for induction of retinoic acid receptor beta, growth inhibition, and apoptosis by retinoic acid in cancer cells. *Mol Cell Biol* **20**, 957–970.

[28] Chen S, Jingjing Y, Ikuko K, Yoshiyuki K, and Zhou D (2005). Positive and negative transcriptional regulation of aromatase expression in human breast cancer tissue. *J Steroid Biochem Mole Biol* **95**, 17–23.

[29] Ham WS, Lee JH, Yu HS, and Choi YD (2008). Expression of chicken ovalbumin upstream promoter-transcription factor 1 (COUP-TF1) in bladder transitional cell carcinoma. *Urology* **72**, 921–926.

[30] Damiao RDS, Oshima CTF, Stavale JN, and Goncalves WJ (2007). Analysis of the expression of estrogen receptor, progesterone receptor and chicken ovalbumin upstream promoter-transcription factor 1 in ovarian epithelial cancers and normal ovaries. *Oncol Rep* **18**, 25–32.

[31] Cooper CS, Nicholson AG, Foster C, Dodson A, Edwards S, Fletcher A, Roe T, Clark J, Joshi A, Norman A, et al. (2006). Nuclear overexpression of the E2F3 transcription factor in human lung cancer. *Lung Cancer* **54**, 155–162.

[32] Foster CS, Falconer A, Dodson AR, Norman AR, Dennis N, Fletcher A, Southgate C, Dowe A, Dearnaley D, Jhavar S, et al. (2004). Transcription factor E2F3 overexpressed in prostate cancer independently predicts clinical outcome. *Oncogene* **23**, 5871–5879.

[33] Feber A, Clark J, Goodwin G, Dodson AR, Smith PH, Fletcher A, Edwards S, Flohr P, Falconer A, Roe T, et al. (2004). Amplification and overexpression of E2F3 in human bladder cancer. *Oncogene* **23**, 1627–1630.

[34] Meyer TD, Bijsmans IT, Van de Vijver KK, Bekaert S, Oosting J, Van Criekinge W, van Engeland M, and Sieben NL (2009). E2Fs mediate a fundamental cell-cycle deregulation in high-grade serous ovarian carcinomas. *J Pathol* **217**, 14–20.

[35] Lu KH, Patterson AP, Wang L, Marquez RT, Atkinson EN, Baggerly KA, Ramoth LR, Rosen DG, Liu J, Hellstrom I, et al. (2004). Selection of potential markers for epithelial ovarian cancer with gene expression arrays and recursive descent partition analysis. *Clin Cancer Res* **10**, 3291–3300.

[36] Baba Y, Nosho K, Shima K, Irahara N, Kure S, Toyoda S, Kirkner GJ, Goel A, Fuchs CS, and Ogino A (2009). Aurora-A expression is independently associated with chromosomal instability in colorectal cancer. *Neoplasia* **11**, 418–425.

[37] He L, Yang H, Ma Y, Pledger WJ, Cress WD, and Cheng JQ (2008). Identification of Aurora-A as a direct target of E2F3 during G_2/M cell cycle progression. *J Biol Chem* **283**, 31012–31020.

[38] Reimer D, Hubalek M, Riedle S, Skvortsov S, Erdel M, Conci N, Fiegl H, Muller-Holzner E, Marth C, Illmensee K, et al. (2010). E2F3a is critically involved in epidermal growth factor receptor–directed proliferation in ovarian cancer. *Cancer Res* **70**, 4613–4623.

[39] Youn BS, Kim DS, Kim JW, Kim YT, Kang S, and Cho NH (2008). NM23 as a prognostic biomarker in ovarian serous carcinoma. *Mod Pathol* **21**, 885–892.

[40] Kinugasa Y, Ishiguro H, Tokita Y, Oohira A, Ohmoto H, and Higashiyama S (2004). Neuroglycan C, a novel member of the neuregulin family. *Biochem Biophys Res Commun* **321**, 1045–1049.

[41] Ida M, Shuo T, Hirano K, Tokita Y, Nakanishi K, Matsui F, Aono S, Fujita H, Fujiwara Y, Kaji T, et al. (2006). Identification and functions of chondroitin sulfate in the milieu of neural stem cells. *J Biol Chem* **281**, 5982–5991.

[42] Feinberg AP, Ohlsson R, and Henikoff S (2006). The epigenetic progenitor origin of human cancer. *Nat Rev Genet* **7**, 21–33.

[43] Tone AA, Begley H, Sharma M, Murphy J, Rosen B, Brown TJ, and Shaw PA (2008). Gene expression profiles of luteal phase fallopian tube epithelium from BRCA mutation carriers resemble high-grade serous carcinomas. *Clin Cancer Res* **14**, 4067–4078.

[44] Jazaeri AA, Yee CJ, Sotiriou C, Brantley KR, Boyd J, and Liu ET (2002). Gene expression profiles of BRCA1-linked, BRCA2-linked, and sporadic ovarian cancers. *J Natl Cancer Inst* **94**, 990–1000.

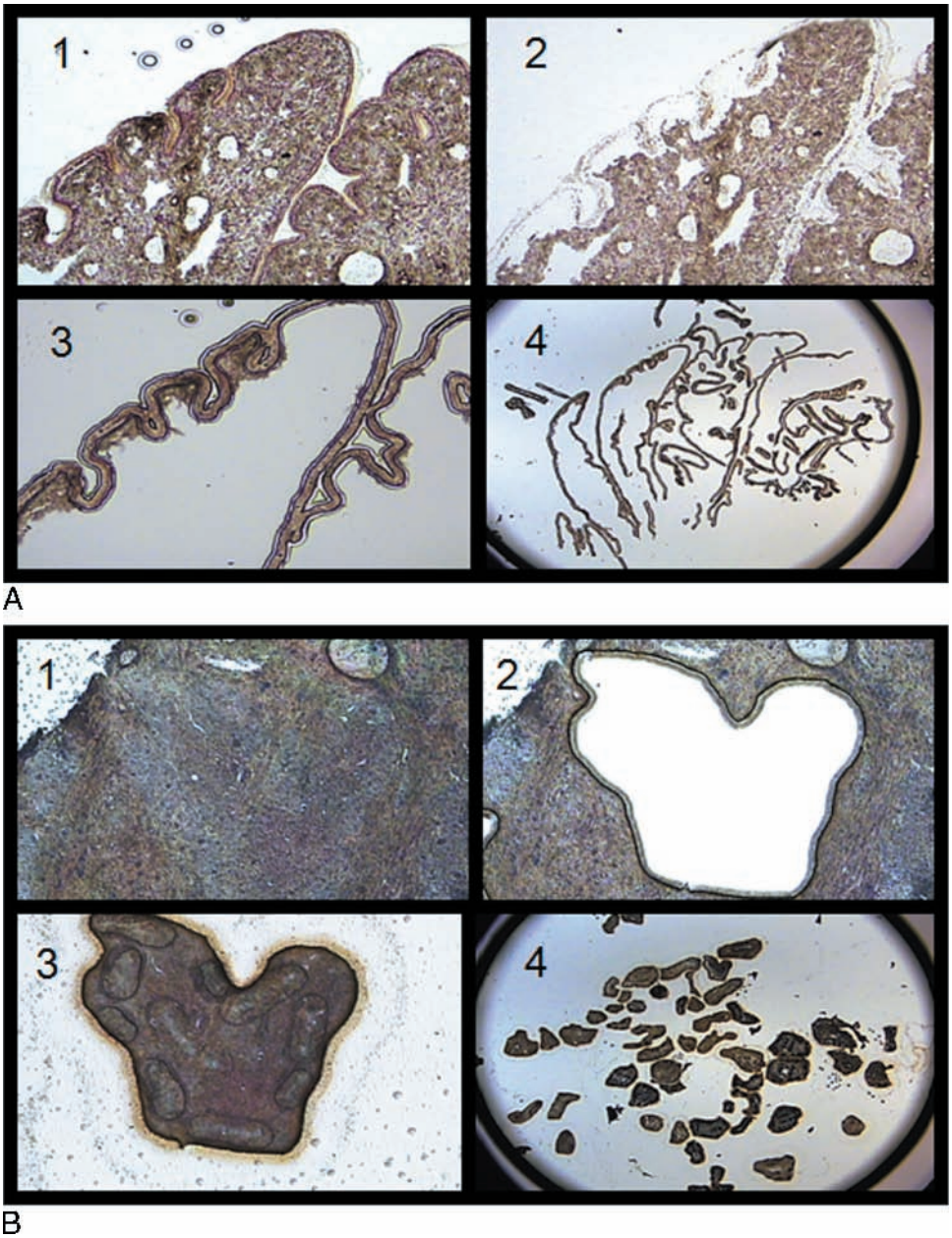

Figure W1. Illustration of LCM. (A) Fallopian tube tissue: (1) fixed slide immediately before performing LCM, (2) slide after LCM and removal of tissue, (3) fallopian tube epithelial tissue adherent to collection cap, and (4) collection cap coated with fallopian tube epithelial tissue at completion. (B) Tumor tissue: same steps (1-4) are shown.

Table W1. Duplicated Samples Used to Interrogate the Gene Expression Signature.

Unique Identifier	Corresponding Case	Tissue Block Used for LCM	BRCA1 Status	Menopausal Status
B1-FTocc no. 1 – DUP	B1-FTocc no. 1	Ipsilateral FT	B1.3109insAA	Pre
B1-FTocc no. 2 – DUP	B1-FTocc no. 2	Contralateral FT	(120A>G)	Post
B1-FTocc no. 6 – DUP	B1-FTocc no. 6	Contralateral FT	B1.C61G	Post

For each of these patients, an independent section of fallopian tube was subjected to RNA isolation, amplification, and array creation.

Table W2. Twelve Additional Fallopian Tube Samples Used to Interrogate the *BRCA1* Preneoplastic Gene Signature.

Case Identifier	Age (years)	Menopausal Status	*BRCA1* Status	Clustering Group
B1-FT no. 1	39	Post	B1.IVS5-11 T>G	WT-FT
B1-FT no. 2	43	Post	B1.C61G	WT-FT
B1-FT no. 3	45	Post	B1.5677insA	B1-FTocc
B1-FT no. 4	46	Post	B1.13+1 G to A	WT-FT
B1-FT no. 5	48	Post	B1.975delAG	WT-FT
B1-FT no. 6	49	Post	B1.3124delA	B1-FTocc
B1-FT no. 7	50	Post	B1.3878insT	WT-FT
B1-FT no. 8	51	Post	B1.Q1200X	B1-FTocc
B1-FT no. 9	52	Post	B1.120A>G(M1V)	B1-FTocc
B1-FT no. 10	53	Post	B1.5385insC	WT-FT
B1-FT no. 11	59	Post	B1.del exon 17	B1-FTocc
B1-FT no. 12	62	Post	B1.R1699W	WT-FT

Each fallopian tube was collected at the time of prophylactic salpingo-oophorectomy from a patient with a known deleterious BRCA1 mutations. None of these samples were used in the derivation of the *BRCA1* preneoplastic gene signature.

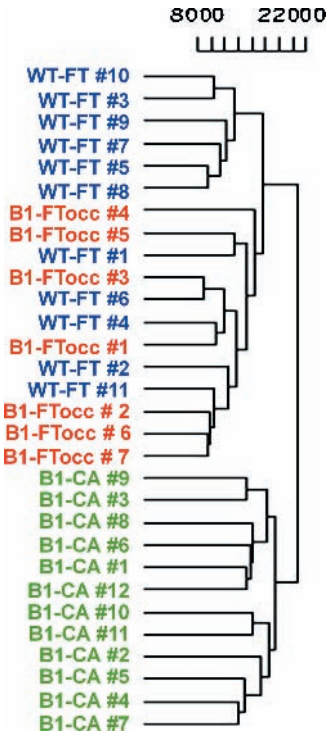

Figure W2. Unsupervised hierarchical clustering of cases using all 18,600 probe sets expressed with adequate quality on the arrays. B1-CA formed a distinct group from the fallopian tube samples.

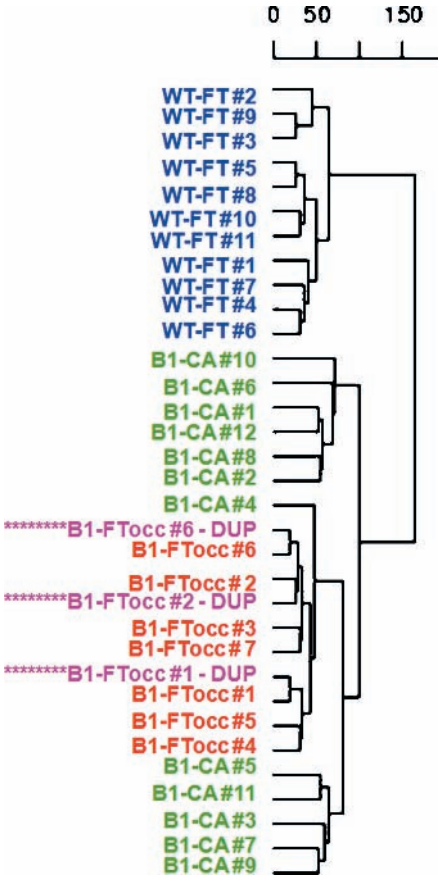

Figure W3. Using the same cases analyzed to create the gene signature, duplicate sections were made, and the protocol was repeated to assess validity. For case no. 1, the ipsilateral FT was used, and for case nos. 2 and 6, the contralateral FT was used. Frozen tissue was subjected *independently* to sectioning, LCM, and RNA amplification. These duplicated samples were then subjected to unsupervised hierarchical clustering using the original 41 probe set gene signature. Clustering of the three duplicated samples (B1-FTocc DUP) shows that duplicates cluster near regardless of whether they are taken from the ipsilateral or contralateral fallopian tube.

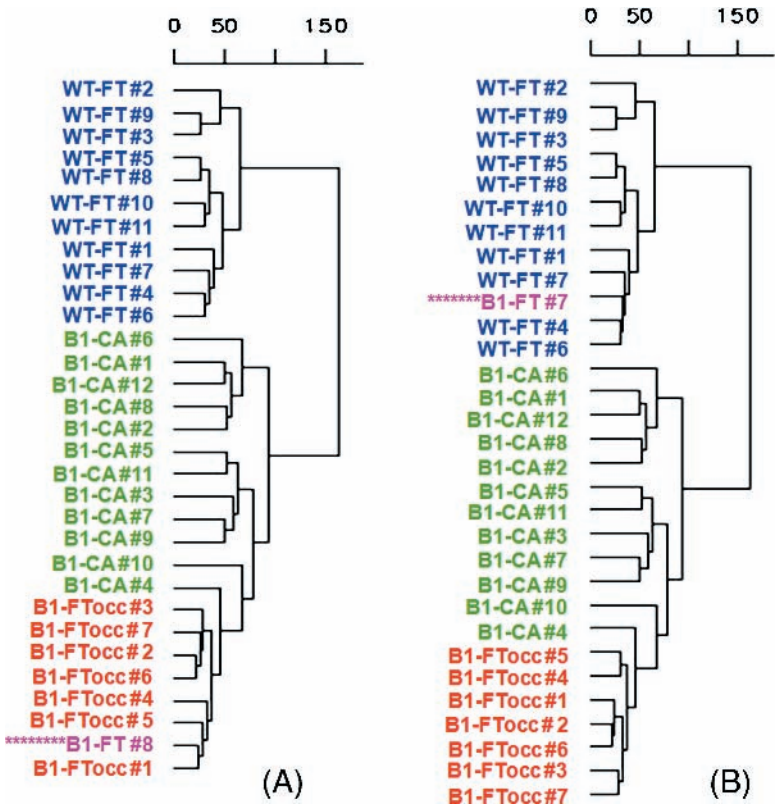

Figure W4. Representative examples of clustering with the independent B1-FT test samples using the 41 probe set gene signature. (A) B1-FT no. 8 clustered with the B1-FTocc/B1-CA group, whereas (B) B1-FT no. 7 clustered with the WT-FT group.